Chapter 1

Theory of neutrino physics

Neutrinos were first theoretically proposed by Wolfgang Pauli [1, 2] as very light electrically neutral particles with a half-integer spin and a possible magnetic moment [3]. They formed a crucial part of Enrico Fermi's successful theory of β decays [4, 5], which solidified their importance in particle physics even before their first experimental detection. Fermi's theory developed into the Standard Model (SM) of particle physics [6–8], which in its current form contains three generations of fermions. Each generation involves two leptons: one charged lepton and one neutrino, which has no mass, nor magnetic moment.

The SM is mathematically described by a Lagrangian, in which neutrinos are represented by a two-component left-handed chiral fields $\nu_{\alpha L}$, where $\alpha = e, \mu, \tau$ denotes the three neutrino generations, also called flavours [9–11]. Neutrino fields form weak isospin doublets $L_\alpha = \begin{pmatrix} \nu_{\alpha_L} \\ \alpha_L \end{pmatrix}$ with their associated left-handed charged lepton fields α_L. Unlike for the charged leptons, there is no right-handed chiral neutrino singlet field in the SM. This means that neutrinos cannot obtain a mass term, since the fermion mass terms arise from the Higgs mechanism [12–14] via the Yukawa coupling of the fermion and the Higgs fields[1] [15], which requires a combination of left-handed and right-handed chiral fields [16]. Additionally, since neutrinos are massless in the SM, all the neutrinos are left-handed helicity particles, and all the antineutrinos ($\overline{\nu}$) are right-handed helicity antiparticles. Therefore, neutrinos and antineutrinos are mutually related not only by a charge conjugation, but by a combined Charge conjugation - Parity (CP) symmetry: $\nu \overset{CP}{\longleftrightarrow} \overline{\nu}$.

The interaction terms for neutrinos can be separated into two parts, describing the Charged Current (CC) interactions with the W_μ gauge field and the Neutral Current (NC) interaction with the Z_μ gauge field, which are coupled to the $W^\pm$ and Z^0 gauge

[1] Further discussion about possible neutrino mass terms in Sec. 1.4

bosons respectively. Neglecting the non-neutrino components, the two neutrino interaction terms are [16]

$$\mathcal{L}_{\text{CC}}^{\text{SM}} = -\frac{g_w}{\sqrt{2}} \sum_{\alpha=e,\mu,\tau} \overline{\nu}_{\alpha L} \gamma^{\mu} \alpha_L W_{\mu}^{+} + \text{h.c. and} \tag{1.1}$$

$$\mathcal{L}_{\text{NC}}^{\text{SM}} = -\frac{g_w}{2\cos(\theta_W)} \sum_{\alpha=e,\mu,\tau} \overline{\nu}_{\alpha L} \gamma^{\mu} \nu_{\alpha L} Z_{\mu}^{0}. \tag{1.2}$$

Here g_w is the weak coupling constant, θ_W is the Weinberg angle and γ^{μ} $(\mu = 0, 1, 2, 3)$ are the four Dirac gamma matrices. The $\overline{\nu}_{\alpha L}$ denotes the Dirac adjoint of $\nu_{\alpha L}$ and h.c. the hermitian conjugate. These two terms describe all the possible SM neutrino interaction vertices. Figure 1.1 shows the CC and the NC interaction of neutrinos and antineutrinos and, in case of the CC diagram, can also be flipped around the vertical axis to show the production of neutrinos from the weak interaction (or decays) of leptons. They can also be rotated $90°$ to either show the annihilation, or the production of the neutrino-lepton (for CC), or neutrino-antineutrino (for NC) pairs.

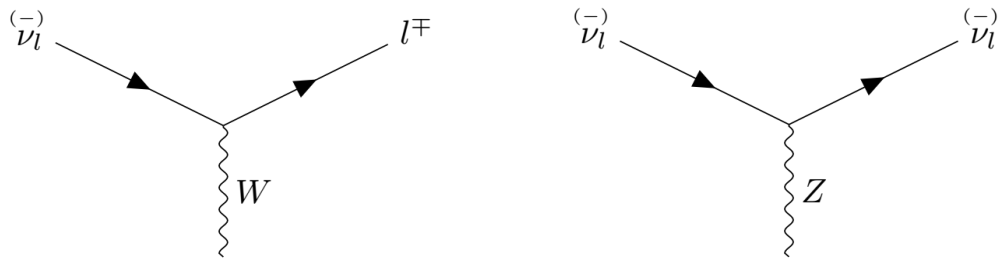

Figure 1.1: Neutrino interaction vertices in the SM via the weak charged currents (left) and the neutral currents (right).

1.1 Neutrino Production

Some of the most common neutrino and antineutrino production channels include nucleon transitions via CC weak interactions. Specifically, the transition of a neutron into a proton, either as the decay of a free neutron, or as the β^{-} decay for neutrons bound in nucleus, produces an electron and an electron antineutrino:

$$n \rightarrow p + e^{-} + \overline{\nu}_e. \tag{1.3}$$

The study of the electron spectrum from β^- decay was the reason Pauli proposed the existence of the neutrino [1]. Additionally, this channel is an abundant source of $\overline{\nu}_e$ from nuclear reactors, which were the first artificial sources of neutrinos, significantly increasing the flux of high energy neutrinos compared to the naturally occurring sources, thus enabling the first ever detection of a neutrino [17–19].

Similarly, the production of an electron neutrino together with a positron via the transition of a proton into a neutron can occur inside the nucleus either as the β^+ decay:

$$p \rightarrow n + e^+ + \nu_e, \tag{1.4}$$

or via the electron capture:

$$p + e^- \rightarrow n + \nu_e. \tag{1.5}$$

This channel occurs in stars and in the first phase of supernovae [16]. However, most supernovae neutrinos are created via a thermal pair production via NC interaction

$$e^- + e^+ \rightarrow \nu_\alpha + \overline{\nu}_\alpha \tag{1.6}$$

producing neutrinos and antineutrinos of all flavours. Neutrino pair production via the decay of Z^0 was studied in great detail [20], since the magnitude of the Z^0 decay width depends on the number of neutrino flavours (N_ν) that can couple to Z^0, with the current best fit $N_\nu = 2.9840 \pm 0082$ [21]. Therefore, there should be exactly three light active neutrino flavours.

An abundant source of ν_μ and $\overline{\nu}_\mu$ is the decay of pions and muons

$$p + X \rightarrow \pi^\pm \rightarrow \mu^\pm + \nu_\mu \left(\overline{\nu}_\mu\right) \tag{1.7}$$

$$\mu^\pm \rightarrow e^\pm + \overline{\nu}_\mu \left(\nu_\mu\right) + \nu_e \left(\overline{\nu}_e\right), \tag{1.8}$$

which naturally occurs in Earth's atmosphere from the interaction of cosmic ray protons. It is notable, that if all the muons decay by the time they reach Earth's surface, the ratio of $(\nu_\mu + \overline{\nu}_\mu) : (\nu_e + \overline{\nu}_e)$ should be exactly 2:1. The same process is also used in the modern accelerator-based neutrino sources, which use protons from accelerators with desired energies, impinge them onto a fixed target, and focus the resulting hadrons (mostly π) to achieve a highly pure and precise source of ν_μ or $\overline{\nu}_\mu$ [22, 23].

Heavier hadrons, such as kaons and charmed particles, can be produced from accelerated protons and other particles, either from natural or artificial origins. These hadrons then also produce neutrinos, including ν_τ and $\overline{\nu}_\tau$ if their energies are high enough [24, 25].

1.2 Neutrino Interactions

The interaction of neutrinos with matter can either be categorized based on the target, which is generally either an atomic electron or a nucleus, or the neutrino energy.

Neutrino-electron interactions occur either via elastic scattering, which result in a neutrino and an electron, or via the inverse muon (or tau) decay, which contains a muon (or tau) in the final state. Both of these interactions at the lowest order involve only free leptons and are very well understood theoretically. The elastic scattering has no energy threshold and can occur for any neutrino. On the other hand, due to the large difference between m_e and m_μ/m_τ, the inverse muon decay has an energy threshold of $E_{\nu_\mu} > 10.92\,\mathrm{GeV}$, and the inverse tau decay $E_{\nu_\tau} > 3\,\mathrm{TeV}$ [16, 26].

Neutrino-nucleus interactions can be, to an extent, approximated by the interaction of a neutrino with quasi-free nucleons inside the nucleus [27]. These interactions can be separated into different interaction channels based on what happens to the nucleon and therefore on the resulting particles. The interaction channels depend on the neutrino incident energy, as illustrated on the case of ν_μ CC interactions in Fig. 1.2.

At lower energies, neutrino-nucleon interactions result in the production of either a nucleon together with a neutrino in the case of NC elastic scattering, or a nucleon with a charged lepton in the case of CC Quasi-Elastic (QE) interactions. The CCQE interaction of an antineutrino on a proton

$$\overline{\nu}_\alpha + p \to n + \alpha^+ \tag{1.9}$$

is called the inverse β decay and was used for the first ever detection of neutrinos (specifically $\overline{\nu}_e$ from a nuclear reactor) [17, 18]. Together with the interaction of a neutrino on a neutron

$$\nu_\alpha + n \to p + \alpha^- \tag{1.10}$$

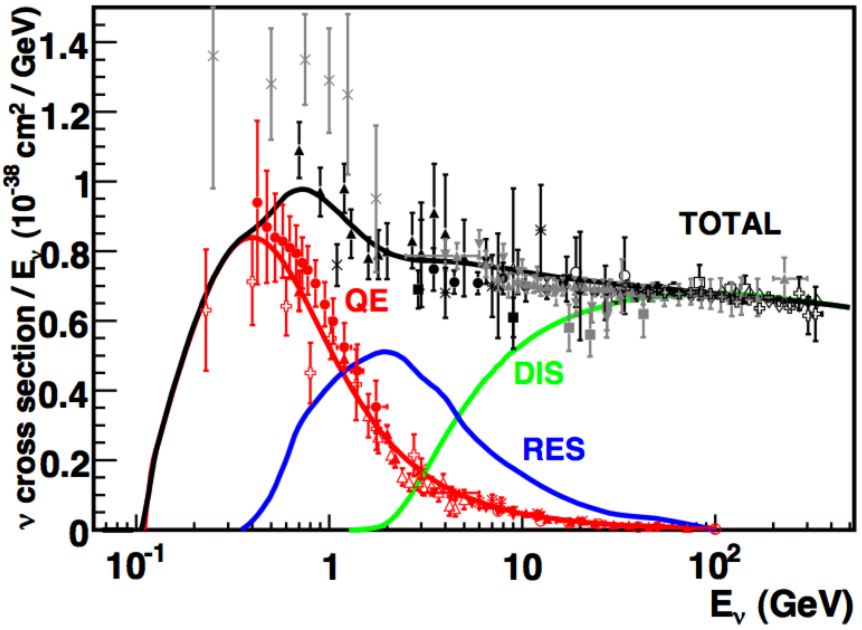

Figure 1.2: Neutrino CC cross sections on an isolated nucleon divided by the neutrino energy based on the interaction types: Quasi-Elastic (QE), Resonant baryon production (Res) and Deep Inelastic Scattering (DIS). Figure is from [28] and compares the measured data [27] and the prediction provided by the NUANCE generator [29].

they serve as fundamental processes for neutrino detection [24, 30, 31]. There is no low energy threshold for the ν_e CCQE interaction, however, there is a threshold for $\overline{\nu}_e$: $E_{\overline{\nu}_e} \gtrsim 1.8\,\mathrm{MeV}$ and for the other neutrino and antineutrino flavours: $E_{\nu_\mu} \gtrsim 110\,\mathrm{MeV}$ and $E_{\nu_\tau} \gtrsim 3.5\,\mathrm{GeV}$.

At higher energies, neutrinos can transfer enough energy to the outgoing nucleon to excite it into a resonant baryon, which then decays back into the original nucleon and into one or more additional particles. This Resonant baryon production (Res) has a threshold of about $270\,\mathrm{MeV}$ for ν_μ and can be distinguished by the presence of an additional π on top of the CCQE products, or, at higher energies, even of multiple additional π's or other hadrons. Increasing the neutrino incident energy even higher means that neutrinos can start probing the quark contents of the individual nucleons in the Deep Inelastic Scattering (DIS), as can be seen in Fig. 1.2.

Even though the approximation of nuclei as collections of quasi-free nucleons is useful, it has been shown [32] there are important nuclear effects that have to be considered. For example the Fermi motion of nucleons and their binding inside the nucleus, or Pauli's exclusion principle resulting in nucleon energy levels [33]. Another important example is the two particle - two hole (2p2h) interaction [34–36],

which occurs when neutrinos interact with a correlated pair of nucleons and can significantly increase the QE cross section [33]. The 2p2h interaction often occurs via the Meson Exchange Current (MEC), where the meson effectively propagates the interaction between the two correlated nucleons. Furthermore, the products of all of the aforementioned interactions can re-interact inside of the nucleus in Final State Interactions (FSIs), which can alter the particle content observed in the detector.

Additionally, if the total energy transferred to the nucleus is small neutrinos can interact with the entire nucleus coherently, where the contributions from each individual nucleon are added together. At low energies, neutrinos can interact via the Coherent Elastic ν-Nucleus Scattering (CEvNS) [37], which results in the excitation of the nucleus. At higher energies, neutrinos can interact via the Coherent π (COHπ) production, which produces a single π without transferring much momentum to the nucleus. In case of the NCCOHπ production the produced π is neutral and for the CCCOHπ there is an additional charged lepton and the produced π is positive (negative) for (anti)neutrinos. As the produced π receives most of the transferred momentum from the neutrinos, it generally travels in the same direction as the initial neutrino and can be difficult to distinguish, especially from e and γ signals in a detector [33].

1.3 Neutrino Oscillation

The idea that neutrinos can oscillate originates as a possibility of transitions between neutrinos and antineutrinos [38, 39], analogically to the already known oscillations of $K^0 \leftrightarrow \overline{K^0}$. This was adapted to the oscillations between different neutrino flavours [40, 41], by considering that the flavour neutrino states ν_α, which are the eigenstates of weak interactions described in Eq. 1.1 and 1.2, are not identical to the mass neutrino states ν_k, which are the eigenstates of the vacuum Hamiltonian $\mathcal{H}_0$:

$$\mathcal{H}_0 \left|\nu_k\right\rangle = E_k \left|\nu_k\right\rangle, k = 1, 2, 3, ..., \tag{1.11}$$

with energy E_k. Instead, the neutrino flavour and mass eigenstates are related as

$$\left|\nu_\alpha\right\rangle = \sum_k U^*_{\alpha k} \left|\nu_k\right\rangle, \tag{1.12}$$

where U is the Pontecorvo-Maki-Nakagawa-Sakata (PMNS) matrix, named after the authors [16, 42]. U is defined as unitary, which makes the inverse relation simply

$$|\nu_k\rangle = \sum_\alpha U_{\alpha k} |\nu_\alpha\rangle . \tag{1.13}$$

Using the Schrödinger equation

$$i\frac{d}{dt} |\nu_k(t)\rangle = \mathcal{H} |\nu_k(t)\rangle , \tag{1.14}$$

the evolution of massive neutrino states in vacuum ($\mathcal{H} = \mathcal{H}_0$) can be described by plane waves

$$|\nu_k(t)\rangle = e^{-iE_k t} |\nu_k\rangle . \tag{1.15}$$

The energy of a neutrino state with mass m_k and momentum $\overrightarrow{p}$

$$E_k = \sqrt{\overrightarrow{p}^2 + m_k^2} \tag{1.16}$$

can be approximated as

$$E_k \xrightarrow{m^2 \ll p^2 \approx E^2} E + \frac{m_k^2}{2E}, \tag{1.17}$$

assuming small neutrinos masses and for ultra-relativistic neutrinos [16]. Additionally, as it is generally easier to measure the distance neutrinos travel (L), rather than the time (t), and given the notation $c \equiv 1$, where c is the speed of light in vacuum, it is common to interchange $L \leftrightarrow t$.

Given the orthogonality of neutrino states, $\langle\nu_k|\nu_j\rangle = \delta_{kj}$ and $\langle\nu_\alpha|\nu_\beta\rangle = \delta_{\alpha\beta}$, and using Eq. 1.15, 1.12 and 1.13, the amplitude of the oscillation (transition) from $\nu_\alpha \to \nu_\beta$ over the 'baseline' L can be written as

$$A_{\nu_\alpha \to \nu_\beta}(L) \equiv \langle\nu_\beta|\nu_\alpha(L)\rangle = \sum_k U^*_{\alpha k} U_{\beta k} e^{-iE_k L} \tag{1.18}$$

and the probability as

$$P_{\nu_\alpha \to \nu_\beta}(L) = \left|A_{\nu_\alpha \to \nu_\beta}(L)\right|^2 = \sum_{k,j} U^*_{\alpha k} U_{\beta k} U_{\alpha j} U^*_{\beta j} e^{-i(E_k - E_j)L}. \tag{1.19}$$

Using Eq. 1.17 and by defining the neutrino mass splitting (also called the mass

squared difference) as

$$\Delta m^2_{kj} \equiv m^2_k - m^2_j, \tag{1.20}$$

the oscillation probability can be expressed as

$$P_{\nu_\alpha \to \nu_\beta}(L) = \sum_{k,j} U^*_{\alpha k} U_{\beta j} U_{\alpha j} U^*_{\beta j} e^{-i \frac{\Delta m^2_{kj} L}{2E}}. \tag{1.21}$$

So far no assumption has been made as to the specific number of neutrino mass or flavour states. However, as was described above in Sec. 1.1, from the decay of Z^0 we know there are probably exactly three active neutrino flavour states, ν_e, ν_μ and ν_τ. Consequently, it is common to also consider exactly three neutrino mass states. This is often called the three neutrino paradigm. Therefore, the PMNS matrix can be written as [16]:

$$U = \begin{pmatrix} U_{e1} & U_{e2} & U_{e3} \\ U_{\mu 1} & U_{\mu 2} & U_{\mu 3} \\ U_{\tau 1} & U_{\tau 2} & U_{\tau 3} \end{pmatrix} =$$

$$= \begin{pmatrix} 1 & 0 & 0 \\ 0 & c_{23} & s_{23} \\ 0 & -s_{23} & c_{23} \end{pmatrix} \begin{pmatrix} c_{13} & 0 & s_{13} e^{-i\delta} \\ 0 & 1 & 0 \\ -s_{13} e^{i\delta} & 0 & c_{13} \end{pmatrix} \begin{pmatrix} c_{12} & s_{12} & 0 \\ -s_{12} & c_{12} & 0 \\ 0 & 0 & 1 \end{pmatrix}, \tag{1.22}$$

where $c_{ij} \equiv \cos\theta_{ij}$ and $s_{ij} \equiv \sin\theta_{ij}$. The matrix is parametrized using three mixing angles θ_{12}, θ_{13} ,and θ_{23} and one phase[2], often denoted δ_{CP}. This phase describes a possible CP symmetry violation in neutrino oscillations, which would result in a difference between the neutrino and antineutrino oscillation probabilities.

When neutrinos pass through matter, their evolution changes due to coherent elastic CC and NC scattering. However, since the NC scattering affects all neutrino flavours equivalently, it does not have any effect on neutrino oscillations. Additionally, as electrons are the only charged leptons present in matter, only the relative difference between the CC interactions of ν_e and of the other flavours needs to be considered. The effective interaction potential of neutrinos passing through matter

[2]If neutrinos are Majorana particles, they can have two additional phases, which however do not enter into neutrino oscillation probabilities

with an electron density N_e can be written as

$$V_{\mathrm{CC}} = \pm\sqrt{2}G_F N_e. \tag{1.23}$$

Here G_F is the Fermi coupling constant and the plus or minus sign is for neutrinos or antineutrinos respectively. The electron density (and therefore the interaction potential) can change along the neutrino path, as it does in the Sun, which can resonantly increase the probability of oscillations, as described by the Mikheyev-Smirnov-Wolfenstein (MSW) effect [43, 44]. However, in accelerator based experiments, where neutrinos only pass through the surface of the Earth, the N_e can be approximated as a constant.

The effect of neutrinos passing through matter on oscillation probabilities can be expressed as shifts to mixing angles and to mass squared differences, proportional to the V_{CC}. Since the matter effect differs for neutrinos and antineutrinos, it needs to be carefully considered especially for the δ_{CP} measurement, which relies on the comparison of neutrino to antineutrino oscillations [16].

The first experimental signs of neutrino oscillations appeared as an apparent deficit of solar neutrinos compared to their predicted flux [30]. However, due to low confidence in the prediction of the solar neutrino flux, no conclusion could have been drawn. Similarly, experiments measuring atmospheric neutrinos [45–48] saw a disagreement between the measurement and the prediction for the $\nu_\mu : \nu_e$ fraction of the atmospheric neutrino flux. This *atmospheric neutrino anomaly* was finally resolved by the Super-Kamiokande (SK) experiment [49], reporting the first experimental evidence for neutrino oscillations. The *solar neutrino anomaly* was resolved shortly after by the Sudbury Neutrino Observatory (SNO) experiment [50], which compared the NC rate, unaffected by neutrino oscillations, to the rate of CC neutrino interactions. This was proof that solar neutrinos oscillate without reliance on the model of the Sun. This result also confirmed the importance of accounting for the matter effect in neutrino oscillations, especially for the oscillation of solar neutrinos, due to the large matter density in the Sun.

The difference between the frequency of solar neutrino oscillations and that observed in atmospheric neutrinos proves that there are at least two mass splittings governing neutrino oscillations. As a result, there must be at least three separate

neutrino mass states, with at least two of them possessing non-zero masses. This is in direct contradiction to the SM and is to-date the only laboratory-based observation of physics Beyond Standard Model (BSM) [51].

Currently, the three neutrino paradigm of oscillations between three neutrino flavour states via three neutrino mass states is well established [52, 53]. The magnitudes of both the neutrino mass splittings and of two mixing angles, θ_{12} and θ_{13}, are measured within 3%. The third mixing angle θ_{23} is measured to be close to the maximum mixing value of $45°$. However, there are three main questions yet to be determined for neutrino oscillations [51]:

1. What is the sign of the larger neutrino mass splitting? Is the electron neutrino made up of the lightest neutrino mass states (normal ordering), or the heaviest (inverted ordering)?

2. Is $\theta_{23} < 45°$ or $\theta_{23} > 45°$? These two options determine the $\nu_\mu : \nu_\tau$ relative contributions to the neutrino mass states and are also referred to as the upper and the lower octant respectively.

3. Is there CP violation in neutrino oscillations? What is the value of δ_{CP}? If neutrinos oscillate differently than antineutrinos, this could be an important part of the matter-antimatter asymmetry in the Universe.

All three of these questions are jointly investigated in the current Long Baseline (LBL) accelerator neutrino oscillation experiments, namely the NuMI Off-axis ν_e Appearance (NOvA) [54] and the Tokai to Kamioka (T2K) [55] experiments. Both use precise ν_μ and $\overline{\nu}_\mu$ beams, affected by the matter effect, and compare the rates of ν_μ and $\overline{\nu}_\mu$ disappearance and ν_e and $\overline{\nu}_e$ appearance to constrain neutrino oscillation parameters [51]. The same methods will be used in the next generation LBL neutrino oscillation experiments, namely the Deep Underground Neutrino Experiment (DUNE) [56] and the Hyper-Kamiokande (HK) [57] experiment, which should give the final answers to all three neutrino oscillation questions [51].

1.4 Neutrino Mass

The absolute values of neutrino masses are currently not known and cannot be directly measured in neutrino oscillation experiments. However, results from experiments measuring the kinematic distribution of β decays [58], or from cosmology [59], currently set a limit for each neutrino mass to $< 1\,\mathrm{eV}$. This is several orders of magnitude smaller than the charged fermion masses, suggesting that BSM theories which introduce neutrino masses should have a different mechanism for their generation than the one used for the other fermions [52]. Furthermore, in order to introduce neutrino masses into the SM, it is necessary to either add new fields, break the renormalizability of the SM Lagrangian, or do both [42]. Also, massive neutrinos can no longer be described by Weyl spinors

The most straight-forward solution, often called the *minimally extended SM*, is to add the missing right-handed chiral neutrino fields, which would enable neutrino mass generation through Yukawa couplings with the Higgs field. These right-handed fields would however be singlets under all the SM gauge symmetries and would therefore not participate in any of the SM interactions. Neutrinos created by these fields are called *sterile* and could potentially mix with the *active* neutrinos via neutrino oscillations. There are however a few issues with the minimally extended SM. Since the mass generation mechanism is the same as for the charged fermions, there is no theoretical explanation for the relative smallness of neutrino masses. There is also currently no experimental confirmation of oscillations between active and sterile neutrinos [52], although there are some possible indications [60, 61]. Additionally, having to add new fields by hand makes the SM an incorrect description of reality even at low energies. This is an issue, as it is generally believed that SM is at least a good low energy effective theory of a more complex general theory and only breaks down at some New Physics (NP) threshold value Λ_{NP} [62].

Adding new non-renormalizable terms to the SM Lagrangian, which are suppressed by this NP scale as $1/\Lambda_{NP}$, would maintain the renormalizability (and validity) of the SM at energies well below Λ_{NP} [62]. It is possible to create such a term using only the existing SM fields and preserving the SM gauge symmetries, which after spontaneous symmetry breaking generates neutrino mass terms. Additionally, three of the newly generated masses are also suppressed as $1/\Lambda_{NP}$ and belong to

mostly left-handed (active) fields, while the rest are very large ($\sim \Lambda_{NP}$) and belong to mostly sterile neutrinos, which are therefore also called Heavy Neutral Leptons (HNLs). This is called the see-saw mechanism [63] and provides a natural explanation for the smallness of neutrino masses. Furthermore, the large masses of HNL make them more likely to avoid experimental detection. However, neutrinos with masses produced by this mechanism all have to be Majorana particles [64].

If neutrinos are Majorana particles, they are equivalent to their own antiparticles (via charge conjugation). The particles described as antineutrinos in the previous sections are however still different to neutrinos, although for Majorana neutrinos they only differ by parity transformation. Therefore, Majorana neutrinos and antineutrinos can be seen as two different spin states of a two-state 'Majorana particle'. This is in contrast to neutrinos being Dirac particles, which have four independent states (neutrino/antineutrino, each with two independent spin states), same as the other fermions and as in the minimally extended SM [16]. It is possible for neutrinos to be Majorana particles as they have no electric charge. However, all the other additive quantum numbers, including the total lepton number, must vanish for Majorana neutrinos as well. This means that Majorana neutrinos can effectively annihilate with each other, violating the total lepton number by two units.

A sure way of finding out whether neutrinos are Majorana particles or not is an observation of a neutrino-less double β decay [62]. This is currently a subject of an extensive experimental investigation without a concrete conclusion [52]. Neutrinos being Majorana particles does not affect neutrino oscillations, however, other measurements could probe the nature of neutrinos, or possible theories BSM, such as the measurements of the possible neutrino magnetic moment [51].

Chapter 2

Measuring the Muon Neutrino Magnetic Moment

In this analysis, I aim to detect a potential signal of the effective muon neutrino magnetic moment in the NOvA Near Detector (ND). This signal would manifest as an excess of neutrino-on-electron (ν-on-e) elastic scattering interactions at low electron recoil energies, proportional to the value of the effective neutrino magnetic moment, over the SM background. If no significant excess is observed, I will establish an upper limit on the effective muon neutrino magnetic moment.

Detecting the neutrino magnetic moment would provide a definitive evidence of new BSM physics, and measuring its value would help identify the appropriate BSM theory. As current and planned experiments can only detect an anomalously large neutrino magnetic moment, observing such a signature would strongly suggest that neutrinos are Majorana particles and would have significant implications for astrophysics and cosmology [51].

The best model-independent experimental results on the neutrino magnetic moment come from experiments searching for dark matter using xenon-based detectors. These highly sensitive detectors detect solar neutrinos, which are part of the background in dark matter searches but can be reanalyzed for other purposes. In 2020, the XENON1T experiment observed [65] a low energy excess of solar neutrinos, which could correspond to a signal from an anomalously large effective magnetic moment within $\mu_{\nu_\odot} \in (0.14, 0.29) \times 10^{-10} \mu_B$ at $90\,\%$ Confidence Level (C.L.), where $\nu_\odot$ marks solar neutrinos. However, this result was disfavoured by the follow-up XENONnT experiment in 2022 [66], which saw no excess and set the current world-leading limit on neutrino magnetic moment at $\mu_{\nu_\odot} < 0.063 \times 10^{-10} \mu_B$ at $90\,\%$ C.L.. Other solar neutrino experiments also reported null results regarding neutrino magnetic moment [67, 68], placing less stringent limits on its value. Given some basic assumptions [68, 69] this limit for solar neutrinos would correspond to a limit on muon neutrino

effective magnetic moment of $\mu_{\nu_\mu} < 0.137 \times 10^{-10}\mu_B$. However, the relationship between effective magnetic moments of different neutrino flavours may be non-trivial, especially in the context of possible new BSM physics, and studying muon neutrinos remains an important endeavour [70].

The best results for ν_μ and $\overline{\nu}_\mu$ come from accelerator-based stopped pion neutrino sources [71, 72], which also do not observe any low energy excess and provide an upper limit on the effective muon neutrino magnetic moment of $\mu_{\nu_\mu} < 6.8 \times 10^{-10}\mu_B$ at $90\,\%$ C.L. [71]. Stopped pion neutrino sources provide a well-understood beams made up of ν_μ, $\overline{\nu}_\mu$ and ν_e with energies up to $52.8\,\mathrm{MeV}$. Slightly looser limits come from pion decay-in-flight accelerator-based measurements (similar to NOvA)[73, 74], which provide a limit of $\mu_{\nu_\mu} < 8.5 \times 10^{-10}\mu_B$ at $90\,\%$ C.L..

Thanks to the very intense and highly pure beam of muon neutrinos and antineutrinos, and a detector designed for the reconstruction and identification of events with electrons in the final state, NOvA is well-positioned to provide a highly competitive, and possibly even world-leading, measurement (or limit) of the effective muon neutrino magnetic moment. A previous analysis of NOvA ND data for a measurement of the effective muon neutrino magnetic moment was presented in a thesis [75], providing a (statistics-only) limit of $\mu_{\nu_\mu} < 15.8 \times 10^{-10}\mu_B$ at $90\,\%$ C.L..

Additionally, ν-on-e elastic scattering interactions are used in various other analyses in NOvA, specifically in efforts to constrain the neutrino beam prediction [76, 77] and in the search for Light Dark Matter (LDM) [78]. These analyses developed various tools and methods that can be utilized in the search for neutrino magnetic moment.

In this chapter, I will provide an overview of the theory of neutrino electromagnetic interactions in Sec. 2.1, focusing on the effective neutrino magnetic moment and its implications for ν-on-e measurements and other theoretical considerations. In Sec. 2.2, I will discuss the analysis strategy, the signal and background definition, as well as the data and simulation samples and the analysis weights. Following this, Sec. 2.3 will explain the selection of events for this analysis, while Sec. 2.4 will cover the electron recoil energy and angle resolution studies and the choice of binning. Sec. 2.5 will address the relevant systematic uncertainties and Sec. 2.6 will introduce the methods used in the statistical analysis of the measurement. Finally, I will present the results of this analysis in Sec. 2.7 and discuss their implications in Sec. 2.8. Sec-

tion 2.9 will summarise the findings of this analysis.

2.1 Theory of neutrino magnetic moment

As was describe in Sec. 1, neutrinos in the SM are massless and electrically neutral particles. However, even SM neutrinos can have electromagnetic interaction through loop diagrams involving charged leptons and the W boson, covered by the neutrino charge radius [51].

In general BSM theories, considering interactions with a single photon as shown on Fig. 2.1, neutrino electromagnetic interactions can be described by an *effective* interaction Hamiltonian [79]

$$\mathcal{H}_{em}^{(\nu)}(x) = \sum_{k,j=1}^{N} \overline{\nu}_k(x)\, \Lambda_\mu^{kj} \nu_j(x)\, A^\mu(x)\,. \tag{2.1}$$

Here $\nu_k(x)\,, k = 1, ..., N$, are neutrino fields in the mass basis with N neutrino mass states, Λ_μ^{kj} is a general vertex function and $A^\mu(x)$ is the electromagnetic field.

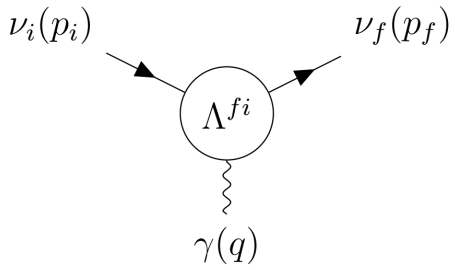

Figure 2.1: Effective coupling of neutrinos with one photon electromagnetic field.

The vertex function $\Lambda_\mu^{fi}(q)$ is generally a matrix and, in the most general case consistent with the SM gauge invariance [80, 81], can be written in terms of linearly independent products of Dirac matrices (γ) and only depends on the four momentum of the photon $(q = p_f - p_i)$:

$$\begin{aligned}\Lambda_\mu^{fi}(q) =& \mathbb{F}_1^{fi}\left(q^2\right) q_\mu + \mathbb{F}_2^{fi}\left(q^2\right) q_\mu\gamma_5 + \mathbb{F}_3^{fi}\left(q^2\right)\gamma_\mu + \mathbb{F}_4^{fi}\left(q^2\right)\gamma_\mu\gamma_5 + \\ & \mathbb{F}_5^{fi}\left(q^2\right)\sigma_{\mu\nu}q^\nu + \mathbb{F}_6^{fi}\left(q^2\right)\epsilon_{\mu\nu\rho\gamma}q^\nu\sigma^{\rho\gamma},\end{aligned} \tag{2.2}$$

where $\mathbb{F}_i^{fi}(q^2)$ are six Lorentz invariant form factors and δ and ϵ are the Dirac delta and the Levi-Civita symbols respectively.

Applying conditions of hermiticity $\left(\mathcal{H}_{em}^{(\nu)\dagger} = \mathcal{H}_{em}^{(\nu)}\right)$ and of the gauge invariance of the electromagnetic field, the vertex function can be rewritten as

$$\Lambda_{\mu}^{fi}(q) = \left(\gamma_{\mu} - q_{\mu}\not{q}/q^2\right)\left[\mathbb{F}_{Q}^{fi}\left(q^2\right) + \mathbb{F}_{A}^{fi}\left(q^2\right)q^2\gamma_5\right] - i\sigma_{\mu\nu}q^{\nu}\left[\mathbb{F}_{M}^{fi}\left(q^2\right) + i\mathbb{F}_{E}^{fi}\left(q^2\right)\gamma_5\right], \tag{2.3}$$

where $\mathbb{F}_{Q}^{fi}, \mathbb{F}_{M}^{fi}, \mathbb{F}_{E}^{fi}$ and $\mathbb{F}_{A}^{fi}$ are hermitian matrices representing the charge, dipole magnetic, dipole electric and anapole neutrino form factors respectively. It is clear that the vertex function only depends on the square of the four momentum of the photon q^2. In coupling with a real photon $(q^2 = 0)$ these form factors become the neutrino charge and magnetic, electric and anapole moments respectively. Additionally, the neutrino charge radius corresponds to the second term in the expansion of the charge form factor [79].

The above expression can be simplified [82] as

$$\Lambda_{\mu}^{fi}(q) = \gamma_{\mu}\left(Q_{\nu_{fi}} + \frac{q^2}{6}\langle r^2\rangle_{\nu_{fi}}\right) - i\sigma_{\mu\nu}q^{\nu}\mu_{\nu_{fi}}, \tag{2.4}$$

where $Q_{\nu_{fi}}$, $\langle r^2\rangle_{\nu_{fi}}$, and $\mu_{\nu_{fi}}$ are the neutrino charge, effective charge radius (also containing anapole moment), and an effective magnetic moment (also containing electric moment) respectively. This is possible thanks to the similar effects of the neutrino charge radius and the anapole moment, and of the neutrino magnetic and electric moments, on neutrino interactions. Therefore, these are the three neutrino electromagnetic properties (charge, effective charge radius and effective magnetic moment) measured in experiments.

The neutrino electric charge is primarily constrained through measurements of the neutrality of matter and cosmological observations, which provide much better constraints than neutrino oscillation experiments [79]. On the other hand, the neutrino charge radius would manifest as an increase in the size of the ν-on-e elastic scattering coupling constants, allowing it to be studied in neutrino oscillation experiments such as NOvA. Additionally, the value of the neutrino charge radius in the SM is only an order of magnitude smaller than the current world-leading limits [52] and measuring it could either confirm the validity neutrino interactions in the SM, or open possibilities to non-standard contributions to neutrino scattering [79]. However, measurement of the neutrino charge radius is not part of this analysis, but may

be included in the future re-analysis of the ν-on-e interactions in the NOvA ND.

2.1.1 Neutrino electric and magnetic dipole moments

The size and effect of neutrino electromagnetic properties depend on the specific BSM theory applied. Evaluating one loop diagrams in the minimally extended SM with three right-handed Dirac neutrinos, as described in Sec. 1.4, gives the first approximation of the electric and magnetic moments, which are now 3×3 matrices with elements:

$$\left.\begin{matrix} \mu^D_{kj} \\ i\epsilon^D_{kj} \end{matrix}\right\} \simeq \frac{3eG_F}{16\sqrt{2}\pi^2}\left(m_k \pm m_j\right)\left(\delta_{kj} - \frac{1}{2}\sum_{l=e,\mu,\tau} U^\star_{lk}U_{lj}\frac{m_l^2}{m_W^2}\right), \tag{2.5}$$

where m_k, m_j are the neutrino masses and m_l are the masses of charged leptons which appear in the loop diagrams [79]. The D superscript denotes Dirac neutrinos and M denotes Majorana neutrinos throughout the section. Also, e is the electron charge, G_F is the Fermi coupling constant, and U is the PMNS neutrino oscillation matrix. Higher order electromagnetic corrections were neglected, but can also have a significant contribution, depending on the theory.

It can be seen that Dirac neutrinos have no diagonal electric moments $\left(\epsilon^D_{kk} = 0\right)$ and their diagonal magnetic moments are approximately

$$\mu^D_{kk} \simeq \frac{3eG_F m_k}{8\sqrt{2}\pi^2} \simeq 3.2 \times 10^{-19}\left(\frac{m_k}{\text{eV}}\right)\mu_B, \tag{2.6}$$

where μ_B is the Bohr magneton which represents the value of the electron magnetic moment [79]. Neutrino magnetic moments are therefore strongly suppressed by the smallness of neutrino masses, with theoretical predictions in Eq. 2.6 several orders of magnitude below the reach of current experiments [82].

The transition magnetic moments in the minimally extended SM from Eq. 2.5 are suppressed with respect to the largest of the diagonal magnetic moments by at least a factor of 10^{-4} due to the m_W^2 in the denominator. The transition electric moments are even smaller due to the mass difference in Eq. 2.5. Therefore an experimental observation of a magnetic moment larger than in Eq. 2.6 would indicate physics beyond the minimally extended SM [79, 83].

Going even further, it is possible [83] to obtain a 'natural' upper limits on the size of the neutrino magnetic moment for any BSM theory that has NP generated at a scale Λ_{NP} as [84]

$$\mu_\nu^D\left(\mu_B\right) \lesssim 3\times 10^{-15}\frac{m_\nu^D\left(\mathrm{eV}\right)}{\left[\Lambda_{NP}\left(\mathrm{TeV}\right)\right]^2}. \tag{2.7}$$

Therefore for $\Lambda_{NP}\simeq 1$TeV (well above the electroweak scale $\Lambda_{EW}\sim 100\,\mathrm{GeV}$) and $m_\nu^D\lesssim 1$eV the limit becomes $\mu_\nu^D\lesssim 3\times 10^{-15}\mu_B$, well below the current experimental capabilities. However, these upper bounds only apply if NP is generated well above the electroweak scale [79].

We need to say that for Majorana neutrinos the magnetic and electric moments are antisymmetric, which implies the different correlation to the mass generation mechanism

[79] Since in the Majorana case the magnetic moment matrix is antisymmetric, it is generated by an antisymmetric magnetic moment operator. On the other hand, the mass matrix and the corresponding mass operator of Majorana neutrinos are diagonal in the mass basis and symmetric in the flavour basis. Therefore, with respect to the Dirac case in which there are no such constraints, additional Yukawa couplings are needed to convert an antisymmetric magnetic moment operator into a symmetric mass operator (Davidson, Gorbahn, and Santamaria, 2005; Bell et al., 2006; Bell, 2007).

[PDG] For Majorana neutrinos the matrix λ is antisymmetric and only transition moments are allowed, while for Dirac neutrinos λ is a general 3×3 matrix.

A minimal extension of the SM that includes Majorana neutrinos requires either addition of a scalar (Higgs) triplet, or right-handed neutrinos together with a Higgs singlet.

TO DO: *Actually write why these values are different for Majorana neutrinos than for Dirac neutrinos* Majorana neutrinos in a minimal extension can be obtained by either adding a $\mathrm{SU}\left(2\right)_L$ Higgs triplet, or right handed neutrinos together with a $\mathrm{SU}\left(2\right)_L$ Higgs singlet [79]. If we neglect the Feynman diagrams which depend on the model of the scalar sector, the magnetic and electric dipole moments are

$$\mu_{kj}^M \simeq -\frac{3ieG_F}{16\sqrt{2}\pi^2}\left(m_k+m_j\right)\sum_{l=e,\mu,\tau}\mathrm{Im}\left[U_{lk}^\star U_{lj}\right]\frac{m_l^2}{m_W^2}, \tag{2.8}$$

$$\epsilon_{kj}^{M} \simeq \frac{3ieG_F}{16\sqrt{2}\pi^2}\left(m_k - m_j\right)\sum_{l=e,\mu,\tau}\mathrm{Re}\left[U_{lk}^{\star}U_{lj}\right]\frac{m_l^2}{m_W^2}. \tag{2.9}$$

These are difficult to compare to the Dirac case, due to possible presence of Majorana phases in the PMNS matrices, but it is clear that they have the same order of magnitude as Dirac transition dipole moments. However, the neglected model dependent contributions can enhance the transition dipole moments [79].

Similar limit for Majorana neutrino magnetic moment would be less stringent than for Dirac neutrinos due to the antisymmetry of the Majorana neutrino magnetic moment form factors TO DO: *Probably explain here a bit more what does this mean*. Considering $m_\nu \lesssim 0.3$eV, the limit can be expressed as

$$\mu_{\tau\mu}, \mu_{\tau e} \lesssim 10^{-9}\left[\Lambda\,(\mathrm{TeV})\right]^{-2} \tag{2.10}$$

$$\mu_{\mu e} \lesssim 3\times 10^{-7}\left[\Lambda\,(\mathrm{TeV})\right]^{-2} \tag{2.11}$$

which is shown in the flavour basis TO DO: *Explain here what is the flavour basis*, which relates to the framework used previously via the PMNS matrix as

$$\mu_{ij} = \sum_{\alpha\beta}\mu_{\alpha\beta}U_{\alpha i}^{\star}U_{\beta j}, \quad \alpha,\beta \in \{e,\mu,\tau\}\,. \tag{2.12}$$

[**?**] ...it is important to notice that the square of the effective MM is independent of the basis chosen (mass/flavour) [255] and it only depends on the neutrino flavour at the source and on its propagation.

TO DO: *Add a discussion about the triangular inequalities* Triangular inequalities also partially described in [**?**]

These considerations imply, that if a magnetic moment $\mu \gtrsim 10^{-15}\mu_B$ would be measured, it is more plausible that neutrinos are Majorana fermions and that the scale of lepton violation would be well below the conventional see-saw scale [83] TO DO: *double check this claim, also reword this sentence*.

[**?**] There is also another important difference between Majorana and Dirac neutrinos for the spin-flavor precession mechanism. For Dirac Neutrinos, the resulting states are right-handed neutrinos which are sterile and therefore undetectable while for Majorana neutrinos spin-flavor precession converts left-handed ν_e into right-handed $\overline{\nu}_\mu$ or $\overline{\nu}_\tau$, which can be detected in accordance with the SNO NC measurement.

[83] Our result implies that an experimental discovery of a magnetic moment near the present limits would signify (i) neutrinos are Majorana fermions and (ii) new lepton number violating physics responsible for the generation of μ_ν arises at a scale Λ which is well below the see-saw scale. In the foregoing analysis, it was convenient to work in the flavor basis (where the charged lepton masses are diagonal)

Effective neutrino magnetic moment

Since experiments detect neutrino flavour states, not the mass states, what we measure is an effective 'flavour' magnetic moment μ_{eff}. μ_{eff} is influenced by mixing of the neutrino magnetic moments (and electric moments) expressed in the mass basis (as described above) and neutrino oscillations TO DO: *This basis relation was already partly described above, mention that and combine the descriptions*. In the ultra-relativistic limit, the neutrino effective magnetic moment is

$$\mu^2_{\nu_l}\left(L, E_\nu\right) = \sum_j \left| \sum_k U^\star_{lk} e^{\mp i \Delta m^2_{kj} L/2E_\nu} \left(\mu_{jk} - i\epsilon_{jk}\right) \right|^2 , \tag{2.13}$$

where the minus sign in the exponent is for neutrinos and the plus sign for antineutrinos [79]. Therefore the only difference between the effective neutrino and antineutrinos magnetic moment is in the phase induced by neutrino oscillations.

For experiments with baselines short enough that neutrino oscillations would not have time to develop ($\Delta m^2 L/2E_\nu \ll\sim 1$), such as the NOvA ND, the effective magnetic moment can be expressed as

$$\mu^2_{\nu_l} = \mu^2_{\overline{\nu}_l} \simeq \sum_j \left| \sum_k U^\star_{lk} \left(\mu_{jk} - i\epsilon_{jk}\right) \right|^2 = \left[U \left(\mu^2 + \epsilon^2\right) U^\dagger + 2\,\mathrm{Im}\left(U\mu\epsilon U^\dagger\right) \right]_{ll'} , \tag{2.14}$$

which is independent of the neutrino energy TO DO: *Figure out how does this relate to the mag moment cross section which does depend on the neutrino energy!*.

TO DO: *Consider if this paragraph is actually important* Since the effective magnetic moment depends on the flavour of the studied neutrino, it is different (but related) for neutrino experiments studying neutrinos from different sources. Additionally some experiments, namely solar neutrino experiments, need to include matter effects on the neutrino oscillations. Therefore the reports on the value (or upper limit)

of the effective neutrino magnetic moment are not directly comparable between different types of neutrino experiments. Theorists publish papers trying to extrapolate the measured effective magnetic moments to each neutrino flavour, but necessarily apply assumptions that might not hold in all BSM theories.

[PDG] Laboratory bounds on λ are obtained via elastic ν-on-e scattering, where the scattered neutrino is not observed. The combinations of matrix elements of λ that are constrained by various experiments depend on the initial neutrino flavor and on its propagation between source and detector (e.g., solar ν_e and reactor $\overline{\nu}_e$ do not constrain the same combinations).

2.1.2 Measuring neutrino magnetic moment

The most sensitive method to measure neutrino magnetic moment is the low energy elastic scattering of (anti)neutrinos on electrons [79]. The diagram for this interaction is shown in Fig. 2.2 displaying the two observables, the recoil electron's kinetic energy ($T_e = E_{e\prime} - m_e$) and the recoil angle with respect to the incoming neutrino beam (θ).

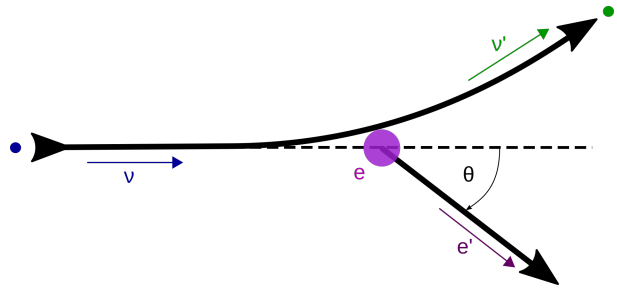

Figure 2.2: Neutrino-on-electron elastic scattering diagram

COMMENT: *Is this derivation too trivial to mention in a thesis? Should I just mention the results? I wanted to have this in the technote, but probably too detailed for a thesis...* TO DO: *Also change all we to passive voice - or should I keep we here?* From simple $2 \to 2$ kinematics we can calculate

$$(P_\nu - P_{e\prime})^2 = (P_{\nu\prime} - P_e)^2 \,, \tag{2.15}$$

$$m_\nu^2 + m_e^2 - 2E_\nu E_{e\prime} + 2E_\nu p_{e\prime} \cos\theta = m_\nu^2 + m_e^2 - 2E_{\nu\prime} m_e. \tag{2.16}$$

Using the energy conservation

$$E_\nu + m_e = E_{\nu'} + E_{e'} = E_{\nu'} + T_e + m_e \Rightarrow E_{\nu'} = E_\nu - T_e \tag{2.17}$$

we get

$$E_\nu p_{e'} \cos\theta = E_\nu E_{e'} - E_{\nu'} m_e = E_\nu \left(T_e + m_e\right) - \left(E_\nu - T_e\right) m_e = T_e \left(E_\nu + m_e\right), \tag{2.18}$$

$$\cos\theta = \frac{E_\nu + m_e}{E_\nu} \sqrt{\frac{T_e^2}{E_{e'}^2 - m_e^2}} = \frac{E_\nu + m_e}{E_\nu} \sqrt{\frac{T_e^2}{T_e^2 + 2T_e m_e}}. \tag{2.19}$$

And finally we get

$$\cos\theta = \frac{E_\nu + m_e}{E_\nu} \sqrt{\frac{T_e}{T_e + 2m_e}}. \tag{2.20}$$

We can rearrange the Eq. 2.20 to get

$$T_e = \frac{2m_e E_\nu^2 \cos^2\theta}{\left(E_\nu + m_e\right)^2 - E_\nu^2 \cos^2\theta}. \tag{2.21}$$

Electron's kinetic energy is therefore kinematically constrained by the energy conservation as

$$T_e \leq \frac{2E_\nu^2}{2E_\nu + m_e}, \tag{2.22}$$

which corresponds to the $\cos\theta \to 1$ when the recoil electron goes exactly forward in the incident neutrino direction.

Considering $E_\nu \sim$ GeV, we can approximate $\frac{m_e^2}{E_\nu^2} \to 0$ and from Fig.2.3 we can see that we can approximate all recoil angles to be very small, therefore $\theta^2 \cong (1 - \cos^2\theta)$. Using Eq.2.20 we get

$$T_e\theta^2 \cong T_e \left(1 - \left(\frac{E_\nu + m_e}{E_\nu}\right)^2 \frac{T_e}{T_e + 2m_e}\right) = T_e \left(1 - \left(1 + \frac{2m_e}{E_\nu}\right) \frac{T_e}{T_e + 2m_e}\right), \tag{2.23}$$

therefore

$$T_e\theta^2 \cong \frac{2m_e T_e}{T_e + 2m_e} \left(1 - \frac{T_e}{E_\nu}\right) = 2m_e \left(\frac{1}{1 + \frac{2m_e}{T_e}}\right) \left(1 - \frac{T_e}{E_\nu}\right), \tag{2.24}$$

and finally

$$T_e\theta^2 \cong 2m_e\left(1-\frac{T_e}{E_\nu}\right) < 2m_e. \tag{2.25}$$

This is a strong limit that clearly distinguishes the ν-on-e elastic scattering events from other similar interaction involving single electron (mainly the ν_eCC interaction).

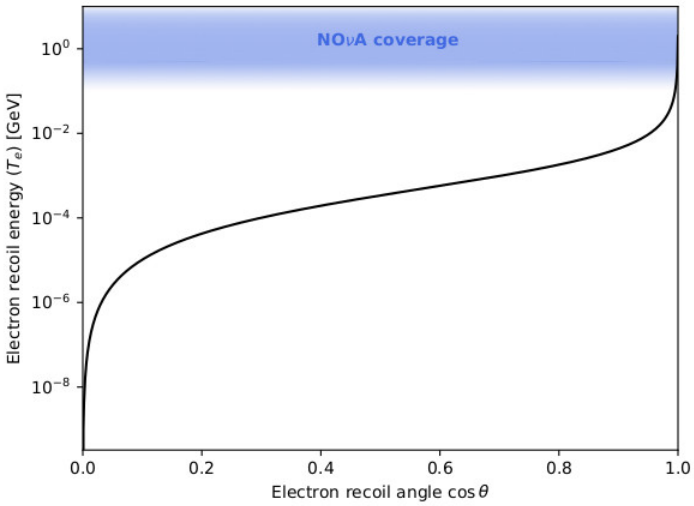

Figure 2.3: Relation between the recoil electron's kinetic energy and angle for ν-on-e elastic scattering. The coverage of the NOvA detectors for measuring the electron recoil energy is shown in blue. Only very forwards electron's are recorded in NOvA.

Neutrino magnetic moment cross section

COMMENT: *Should this only be a subsubsection?* In the ultra-relativistic limit, the neutrino magnetic moment changes the neutrino helicity, turning active neutrinos into sterile TO DO: *cite this properly*. Since the SM weak interaction conserves helicity we can simply add the two contribution to the ν-on-e cross section incoherently [79]:

$$\frac{d\sigma_{\nu_l e^-}}{dT_e} = \left(\frac{d\sigma_{\nu_l e^-}}{dT_e}\right)_{\text{SM}} + \left(\frac{d\sigma_{\nu_l e^-}}{dT_e}\right)_{\text{MAG}}. \tag{2.26}$$

The SM contribution can be expressed as [79]:

$$\left(\frac{d\sigma_{\nu_l e^-}}{dT_e}\right)_{\text{SM}} = \frac{G_F^2 m_e}{2\pi}\left\{(g_V^{\nu_l}+g_A^{\nu_l})^2 + (g_V^{\nu_l}-g_A^{\nu_l})^2\left(1-\frac{T_e}{E_\nu}\right)^2 + \left((g_A^{\nu_l})^2-(g_V^{\nu_l})^2\right)\frac{m_e T_e}{E_\nu^2}\right\}, \tag{2.27}$$

ht

Table 2.1: Neutrino-on-electron elastic scattering total cross sections. TO DO: *Move units to title and add cross sections with thresholds. Also reference this somewhere in text* from Fundamentals of neutrino Physics and Astrophysics, p.139

Process	Total cross section
$\nu_e + e^-$	$\simeq 93 \times 10^{-43} E_\nu \mathrm{cm}^2 \mathrm{GeV}^{-1}$
$\overline{\nu}_e + e^-$	$\simeq 39 \times 10^{-43} E_\nu \, \mathrm{cm}^2 \mathrm{GeV}^{-1}$
$\nu_{\mu,\tau} + e^-$	$\simeq 15 \times 10^{-43} E_\nu \, \mathrm{cm}^2 \mathrm{GeV}^{-1}$
$\overline{\nu}_{\mu,\tau} + e^-$	$\simeq 13 \times 10^{-43} E_\nu \, \mathrm{cm}^2 \mathrm{GeV}^{-1}$

where the coupling constants g_V and g_A are different for different neutrino flavours and for antineutrinos. Their values are:

$$g_V^{\nu_e} = 2\sin^2\theta_W + 1/2, \qquad g_A^{\nu_e} = 1/2, \tag{2.28}$$

$$g_V^{\nu_{\mu,\tau}} = 2\sin^2\theta_W - 1/2, \qquad g_A^{\nu_{\mu,\tau}} = -1/2. \tag{2.29}$$

For antineutrinos $g_A \to -g_A$.

TO DO: *Decide if this is actually useful or not* Using Eq. 2.21 it is possible to get the differential cross section for $\cos\theta$:

$$dT_e = \frac{4m_e E_\nu^2 \left(m_e + E_\nu\right)^2}{\left[\left(m_e + E_\nu\right)^2 - E_\nu^2 \cos^2\theta\right]^2} \cos\theta d\cos\theta \tag{2.30}$$

as

$$\left(\frac{d\sigma_{\nu_l e^-}}{d\cos\theta}\right)_{\mathrm{SM}} = \frac{2G_F^2 E_\nu^2 m_e^2 \cos\theta \left(E_\nu + m_e\right)^2}{\pi\left(\left(E_\nu + m_e\right)^2 - E_\nu^2\cos^2\theta\right)^2} \left\{ \left(g_V^{\nu_l} + g_A^{\nu_l}\right)^2 + \left(g_V^{\nu_l} - g_A^{\nu_l}\right)^2 \left(1 - \frac{2m_e E_\nu \cos^2\theta}{\left(E_\nu + m_e\right)^2 - E_\nu^2\cos^2\theta}\right)^2 + \left(\left(g_A^{\nu_l}\right)^2 - \left(g_V^{\nu_l}\right)^2\right) \frac{2m_e^2\cos^2\theta}{\left(\left(E_\nu + m_e\right)^2 - E_\nu^2\cos^2\theta\right)} \right\}, \tag{2.31}$$

The neutrino magnetic moment contribution is TO DO: *include derivation from [?]* [79]:

$$\left(\frac{d\sigma_{\nu_l e^-}}{dT_e}\right)_{\mathrm{MAG}} = \frac{\pi\alpha^2}{m_e^2}\left(\frac{1}{T_e} - \frac{1}{E_\nu}\right)\left(\frac{\mu_{\nu_l}}{\mu_B}\right)^2, \tag{2.32}$$

where α is the fine structure constant TO DO: *Calculate the total mag moment cross sections*.

Comparison of the SM and the neutrino magnetic moment cross sections is shown on Fig.2.4. Whereas the SM cross section is flat with $T_e \to 0$, the neutrino magnetic moment cross section keeps increasing to infinity. However, this reach is limited by the experimental capabilities of detecting such low energetic neutrinos. Possible NOvA coverage is shown in a shaded blue and it is uncertain we could actually reach as low as 100 MeV TO DO: *Change this claims a little bit*.

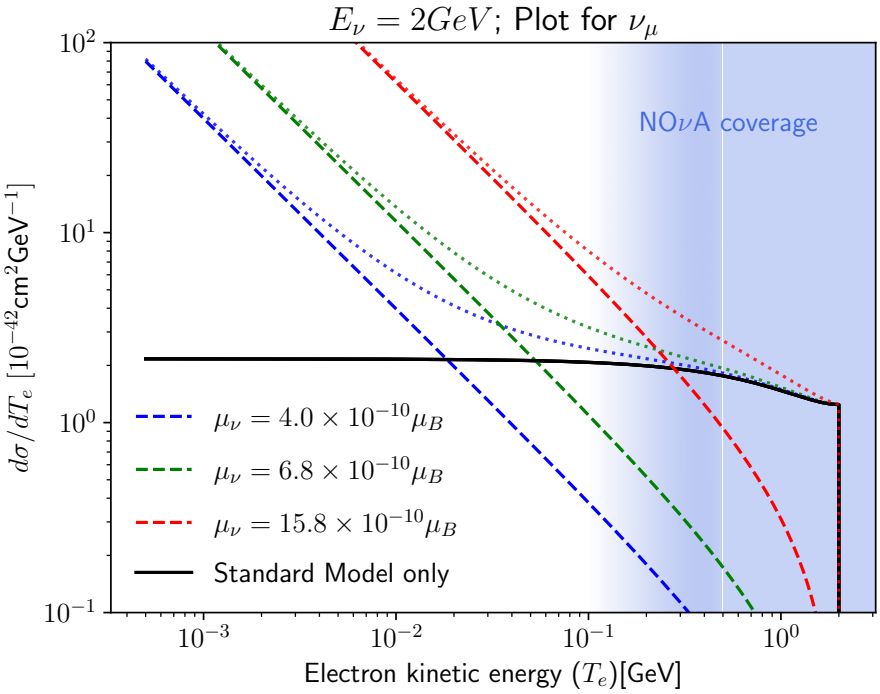

Figure 2.4: Comparison of the neutrino magnetic moment (coloured) and the SM (black) cross sections for the ν-on-e elastic scattering. Different colours depict different values of the neutrino magnetic moment. Dashed lines are the individual cross sections and dotted lines are the added total cross section with the standard model contribution. NOvA coverage of electron recoil energies is shown in shaded blue TO DO: *Reference the colours on the figures to the origins of the values (LSND and Biao).*

As can be seen in Fig. 2.4 and Fig. 2.5, the magnetic moment contribution exceeds the SM contribution for low enough T_e. This can be approximated as [79]:

$$T_e \lesssim \frac{\pi^2\alpha^2}{G_F^2 m_e^3}\left(\frac{\mu_\nu}{\mu_B}\right)^2 \simeq 2.9\times 10^{19}\left(\frac{\mu_\nu}{\mu_B}\right)^2 [\text{MeV}]\,, \tag{2.33}$$

which does not depend on the neutrino energy and makes experiments sensitive to lower energetic electrons more sensitive to the neutrino magnetic moment. This is especially true for the recent dark matter experiments which put stringent limits on

the solar neutrino effective magnetic moment, as described in the following section.

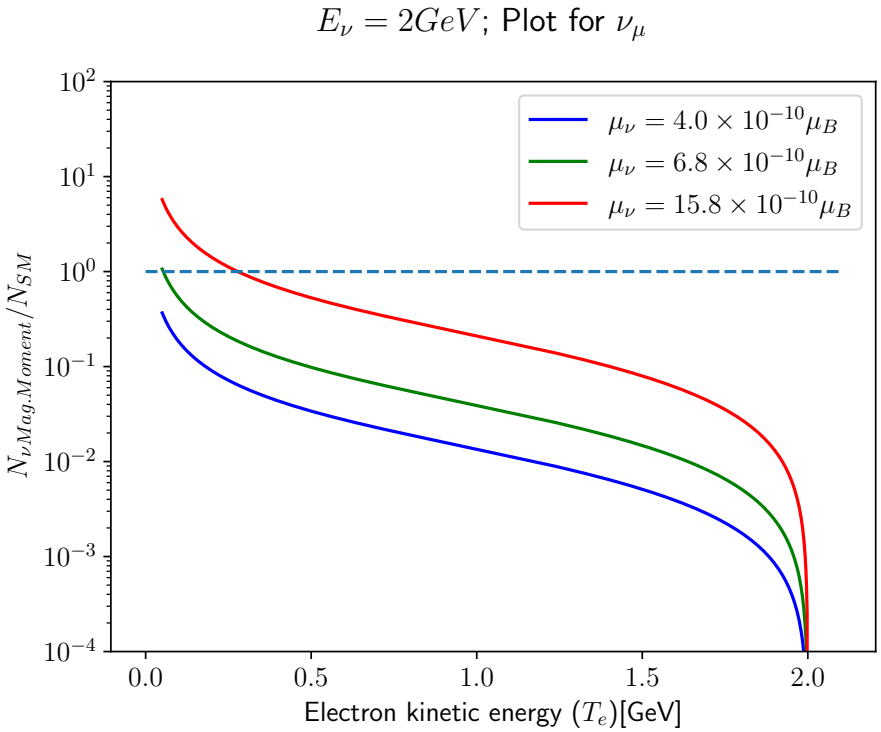

Figure 2.5: Ratio of the neutrino magnetic moment cross section to the SM cross section for the ν-on-e elastic scattering. Different colours depict different effective muon neutrino magnetic moment values.

2.2 Analysis overview

Our analysis strategy is to compare the count of the recorded neutrino events in data with the prediction. The prediction consists of the signal, which is directly related to the value of the neutrino magnetic moment, and the background, which corresponds to the predicted events under the SM. The signal is defined as true ν-on-e events with the neutrino magnetic moment cross section instead of the SM one. Additionally, we require the true vertex to be contained inside of the ND to remove events that originates from outside of the detector. Background is everything else.

The data used in this analysis was collected from the start of the NOvA ND data taking on the 22nd of August 2014, until the 3rd of February 2021. This is the ND data that was used in the latest NOvA neutrino oscillations result [54], with an additional one year of data taking. The ND collected more data since February 2021 which is however still being processed and it is not available at the time of writing this thesis.

The full ND-equivalent exposure of the data sample is approximately 13.8×10^{20} Protons On Target (POT). This exposure is used throughout the rest of this chapter to scale the predicted distributions and number of events. COMMENT: *Should I also talk about the RHC sample here? Future data?*

Maybe also mention something about the data that was excluded - bad runs and bad channels?

This analysis uses the standard NOvA simulation and reconstruction tools, as were discussed in Sec. **??** and **??**. The simulation was created with approximately $4\times$ larger statistics than is available in data to limit statistical uncertainties from simulation. The total exposure for the simulation is approximately 55.4×10^{20} POT. However, for the studies of the systematic uncertainties, only a smaller portion of this full sample is used, specifically 19.3×10^{20} POT ND-equivalent.

The corrections for the known limitations in the simulation are applied in the form of event-by-event analysis weights, which weight each single event based on how it is affected by that particular variation in simulation. To correct for known deficiencies in simulation of neutrino flux or cross sections we apply weights calculated for each event. This includes the external measurements that correct the neutrino beam prediction inside Package to Predict the Flux (PPFX) as described in Sec. **??**, and for the non-ν-on-e background, also the internal and external measurements that constrain the neutrino interaction prediction inside GENIE. These are not applied to the ν-on-e events, as they are assumed to be known precisely from theory. However, the GENIE Monte Carlo (MC) simulation doesn't consider radiative corrections for the ν-on-e events, which are however trivial to implement.

Mention here where did I get the original GENIE cross section from (reference Yiwen's talk or technote, plus the original paper that was used). nu-on-e technote[76]

TO DO: *Write out the actual version of the weight. Including the original and the corrected XSec constants*

MINERvA paper [85]: At tree level, the neutrino-electron scattering cross section is given by... (basically same as I have in the theory) corrected for updated electroweak couplings, CLL and CLR [17] and one-loop electroweak radiative corrections as calculated in Ref. [18]. One deficiency of the calculation of Ref. [18] is that it does not contain the term in the one-loop cross section proportional to CLL

CLR. This deficiency is corrected in a recent calculation [38], and that result is given below. However, as illustrated in Eq. (A1) this term also contains an additional power of m/Enu compared to the terms proportional to C2 LL and C2 LR, and the entire term is therefore negligible at the few-GeV neutrino energies of the MINERvA experiment.

Say that we are not using the third part of the correction because it is tiny and it makes no difference. (tried and tested)

[ND group's technote] In GENIE, the cross section of the nuone elastic scattering signal is calculated at the tree level. To improve the precision of the simulated nuone elastic scattering cross section, we performed radiative corrections to the GENIE nuone elastic scattering as shown in Appendix A. The precision of the simulated nuone elastic scattering cross section is improved by tuning CLL and CLR to one-loop values obtained from global fits to electroweak data 14 and 2. The radiative correction also includes additional low-energy terms in the expression of differential cross section of nuone elastic scattering. In comparison, the neutrino interactions in the NOvA detector are simulated using the GENIE neutrino event generator, where the Weinberg Angle is 0.501716712132. After radiative corrections, the total number of nuone elastic scattering increases 0.83% from the standard GENIE MC.

TO DO: *correct the equation* Calculated as

$$weight_{\text{Radiative Corr.}} = \left.\frac{d\sigma_{\nu-on-e}}{dy}\right|_{\text{Radiative Corr.}} / \left.\frac{\mathrm{d}\sigma_{\nu-on-e}}{\mathrm{d}y}\right|_{\text{GENIE 3}} ; y = \frac{E_e - m_e}{E_\nu} \quad (2.34)$$

TO DO: *What does this do and why does it work? Reference the theory part as to why is the magnetic moment signal simply a rescaling of the GENIE cross section.*

Using the same tree-level cross section from GENIE as in the rad. corr. weight.

TO DO: *Write the name of the weight in CAFAna/nuone namespace and where it is located*

TO DO: *correct the equation* Calculated as

$$weight_{\nu \text{ Mag. Moment}} = \left.\frac{d\sigma_{\nu-on-e}}{dy}\right|_{\nu \text{ Mag. Moment}} / \left.\frac{\mathrm{d}\sigma_{\nu-on-e}}{\mathrm{d}y}\right|_{\text{GENIE 3}} ; y = \frac{E_e - m_e}{E_\nu} \quad (2.35)$$

Due to the relatively low cross section of the ν-on-e interaction, the nominal simulation sample contains too few ν-on-e events, which could result in a significant statistical uncertainty from simulation. To avoid this, we created a ν-on-e-enhanced

simulation sample which contains mainly ν-on-e events with a little non-ν-on-e background overlaid on top to properly account for the possible reconstruction effects of the pileup of neutrino interactions in one spill [76]. In the real detector, the hits from the true ν-on-e interaction can be clustered to another interaction, or additional hits can be clustered together into the ν-on-e event. The total exposure of the ν-on-e-enhanced sample is 1.72×10^{24} POT. To save up on unnecessary disk space and processing usage, the enhanced ν-on-e sample does not include any cross section related parameters and variables, as the ν-on-e interaction is assumed to be known exactly from theory.

The cross section tuning procedure in NOvA (Sec. **??**) applies large weights to MEC events in some parts of the parameter space. However, after the full event selection described below in Sec. 2.3 there is only a small amount of MEC events, specifically ν_eCC MEC events, left in the detector. Applying large tuning corrections to only a small number of events results in large statistical fluctuations. To avoid this, we created another special sample with enhanced number of ν_eCC MEC events. We followed the same procedure as for the ν-on-e-enhanced sample, resulting in the final exposure of 1.99×10^{24} POT.

The summary of the simulation samples and analysis weights for the three different types of signal and background component is shown in Tab. 2.2.

Table 2.2: Overview of the simulation samples and analysis weight used for the different signal and background components.

Signal type	Sample	Weight
Signal	Enhanced ν-on-e	Flux & ν Mag. Moment
ν-on-e background	Enhanced ν-on-e	Flux & Rad. Corr.
ν_eCC MEC background	Enhanced ν_eCC MEC	Flux & Cross Sec.
Other background	Nominal ND	Flux & Cross Sec.

2.3 Event selection

We are searching for ν-on-e elastic scattering events, characterised by a single very forward going electron shower, specifically focusing on low electron recoil energies. The main background for our analysis come from ν_eCC interactions, which produce

electron with an additional activity, and interactions that produce π^0, which decays into two photons producing electromagnetic showers, where each can look similar to the ν-on-e signal. Additionally, there are ν_μCC interactions, which are generally easy to identify from our signal, however their very high abundance in the NOvA ND makes them a dominant background nevertheless.

We explain the motivation behind each cut of the event selection and discuss their effect on the neutrino magnetic moment events below. We also consider possible improvements to the event selection for a future (re-)analysis.

The strategy for event selection is as follows. First, we remove events that failed reconstruction or data collection. Then, we apply pre-selection cuts that remove obvious background. The exact cut is selected by limiting the reduction of the signal efficiency to about $0.25\,\%$. Following this, we apply the containment cuts that remove events that are either not fully contained within the detector, or events that originate from outside of the detector, such are rock muons. Afterwards, we consider several variables that could be used for the signal selection and evaluate their combined performance for a signal selection. We choose cut values that result in the best statistical significance, based on a chosen Figure Of Merit (FOM). Given that we are searching for a very limited number of signal events on top of a large background, we chose a simple statistics-only FOM

$$\text{FOM} = \frac{\text{Signal}}{\sqrt{\text{Background}}}. \tag{2.36}$$

The summary of the cut values for the event selection of neutrino magnetic moment signal is presented in Tab. 2.3, showing the label for the event selection variable, its description and the cut value chosen. These event selection in total reduces signal $44.51\,\%$, ν-on-e background $70.40\,\%$ and other background $99.97\,\%$. After the full event selection, the predicted number of signal events for $\mu_\nu = 10^{-9}\mu_B$ is 23.31 and the total number of background events under the SM hypothesis is 678.26. The most likely improvement is in probing the low energetic events and making sure they make sense. Additionally, it is possible to use a specially designed control regions to mitigate the very high non-ν-on-e background.

2.3.1 Data Collection Quality

To ensure good data quality, we apply the following criteria to data only. These involve the the spill time cut, at least 2^{12} POT per spill, the current in the focusing horn within $-202\,\mathrm{kA} < I_{Horn} < -196.4\,\mathrm{kA}$, position of the beam is within $\pm 2\,\mathrm{cm}$ in both

Table 2.3: Summary of the cut values for the event selection of neutrino magnetic moment signal showing the label for the event selection variable, its description and the cut value chosen. COMMENT: *Should I include the loose cuts here even when they were made stricter during TMVA?*

Label	Description	Cut
Valid Vtx	Valid reconstructed vertex	> 0
N^o Prongs	Number of reconstructed prongs	> 0
Hits / Plane	Number of hits per plane	< 5
Low E_{Shower}	Low cut on calorimetric energy of the most energetic shower	$> 0.5\,\mathrm{GeV}$
N^o Hits Loose	Preliminary cut on the total number of hits for all prongs in a slice	< 200
Prong Length	Length of the longest prong	$< 540\,\mathrm{cm}$
$E\theta^2$ **Loose**	Preliminary cut on the product of the calorimetric energy and angle squared of the leading shower	$< 0.05\ \mathrm{GeV} \times \mathrm{rad}^2$
High E_{Shower} **Loose**	Preliminary upper cut on the calorimetric energy of the most energetic shower	$< 5.5\,\mathrm{GeV}$
Fiducial	Vertex x position	$> -177\,\mathrm{cm}$ $< 177\,\mathrm{cm}$
	Vertex y position	$> -177\,\mathrm{cm}$ $< 177\,\mathrm{cm}$
	Vertex z position	$> 50\,\mathrm{cm}$ $< 1050\,\mathrm{cm}$
Containment	Minimum hit position in x	$> -177\,\mathrm{cm}$
	Maximum hit position in x	$< 177\,\mathrm{cm}$
	Minimum hit position in y	$> -185\,\mathrm{cm}$
	Maximum hit position in y	$< 177\,\mathrm{cm}$
	Minimum hit position in z	$> 55\,\mathrm{cm}$
	Maximum hit position in z	$< 1270\,\mathrm{cm}$
E_{Shower}/E_{Tot}	Fraction of energy contained in the most energetic shower	> 0.91
N^o Hits	Total number of hits for all prongs in a slice	< 116
High E_{Shower}	Calorimetric energy of the most energetic shower	$< 1.4\,\mathrm{GeV}$
ν**-on-e ID**	Convolutional Visual Network (CVN)-based ν-on-e identifier	> 0.65
$E\pi^0$ **ID**	CVN-based ν-on-e and π^0 identifier	> 0.63
$E\theta^2$	Product of the calorimetric energy and angle squared of the leading shower	$< 0.0048\ \mathrm{GeV} \times \mathrm{rad}^2$

x and y axis and that the width of the beam is within 0.57 and $1.58\,\mathrm{cm}$. Additionally, we remove events that are incomplete, or with problems in one or more Data Concentration Modules (DCMs). TO DO: *Reference the 3f data quality technote*

2.3.2 Reconstruction Quality

Since electron are reconstructed by slicing, then vertexing, then reconstructing prongs. To identify electron we request that there is a valid reconstructed vertex and at least one reconstructed prong. Even though electrons only consist of a single shower, we don't reject events with more than one prongs in a slice, as the reconstruction can wrongly assign noise hits as a separate prong. We do not want to reject these events as we might still recover the true signal event from there.

Figure 2.6 and Tab. 2.4 show that about $67\,\%$ signal events do not have a valid reconstructed vertex. This is due to the concentration of the signal events at very low electron recoil energies, which can often consist of a single hit or only a few hits. As can be seen in the bottom plot of Fig. 2.6, events with small true electron recoil energy have much smaller vertex reconstruction efficiency than higher energetic electrons. However, improving NOvA vertex reconstruction at low energies might significantly aid the search for the neutrino magnetic moment. Ongoing work is improving the vertex reconstruction by using Machine Learning (ML) approach instead of the currently used Hough transform together with Elastic Arms [86].

Additionally, we're placing a cut on the number of hits per plane to < 5. This is to remove the so-called 'Front End Board (FEB) flashers', which are caused by a very high energy deposit in one cell, such that it affects all the other channel on the same Avalanche Photodiode (APD) [87]. The cut value was chosen so that it removes $\leq 0.25\,\%$ signal events, which is the same criterion as is used for the basic event selection cuts described below. Relative comparisons between signal and background for the number of prongs and the number of hits per plane are shown in Fig. 2.7.

COMMENT: *Already applying the cut here to help reduce the events for TMVA. This cut is based purely on reco quality (we don't trust events below 0.5GeV, especially not for the CVN nuone ID variables*

TO DO: *discuss the energy cut, should this be removed? What is the effect on the event count? Why was this included in the first place (the identifiers are not as strong*

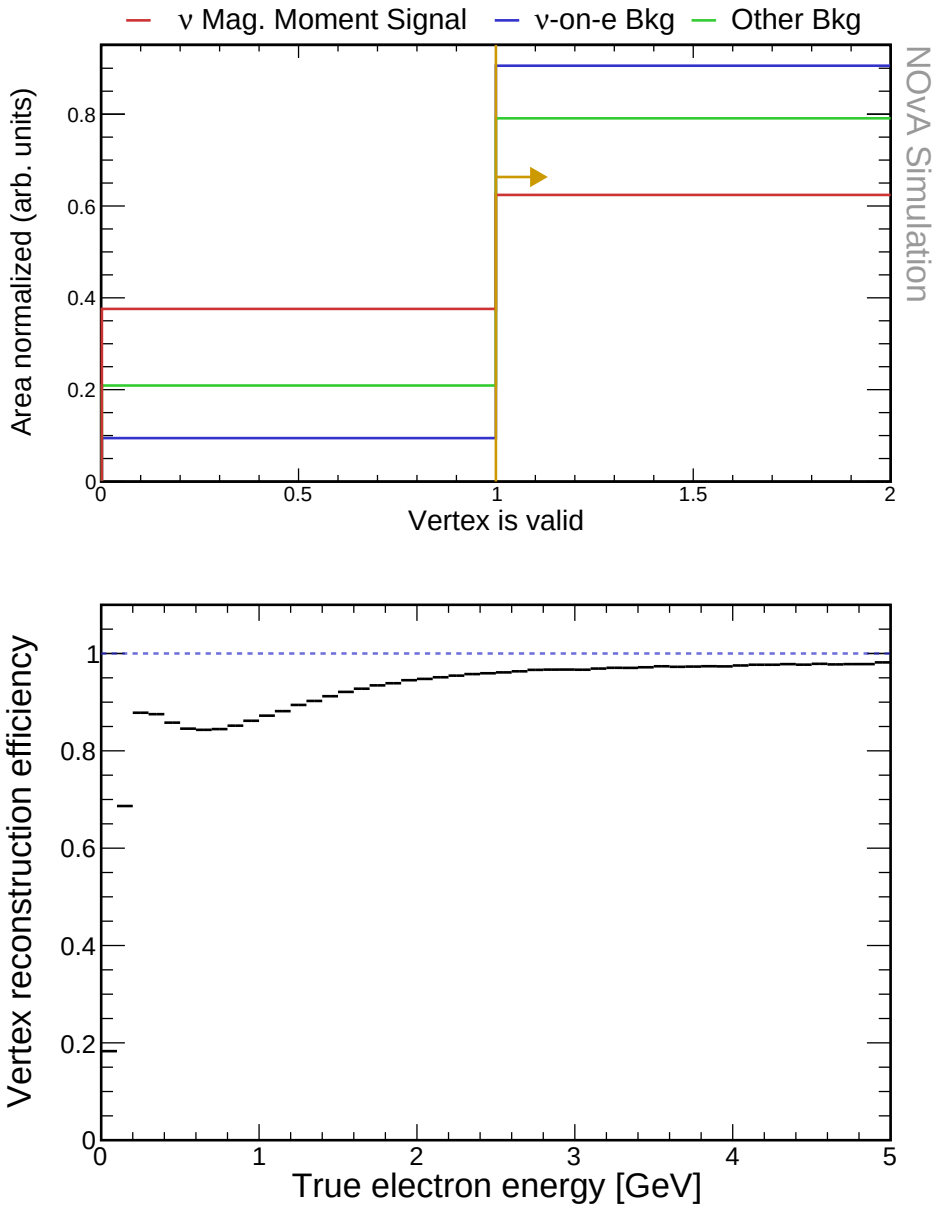

Figure 2.6: Top: Relative comparison of the signal (red), ν-on-e background (blue), and other background (green) events for the vertex reconstruction quality selection. Each histogram is area-normalised and the first bin corresponds to events without a valid vertex and second bin to events with correctly reconstructed vertex. The yellow line indicates the chosen cut value: all events have to have a valid reconstructed vertex. Bottom: profile histogram of the 'vertex is valid' variable as a function of the true electron energy for the true signal events, showing the significant drop in vertex reconstruction efficiency at low electron recoil energies. No selection was applied prior to making these plots.

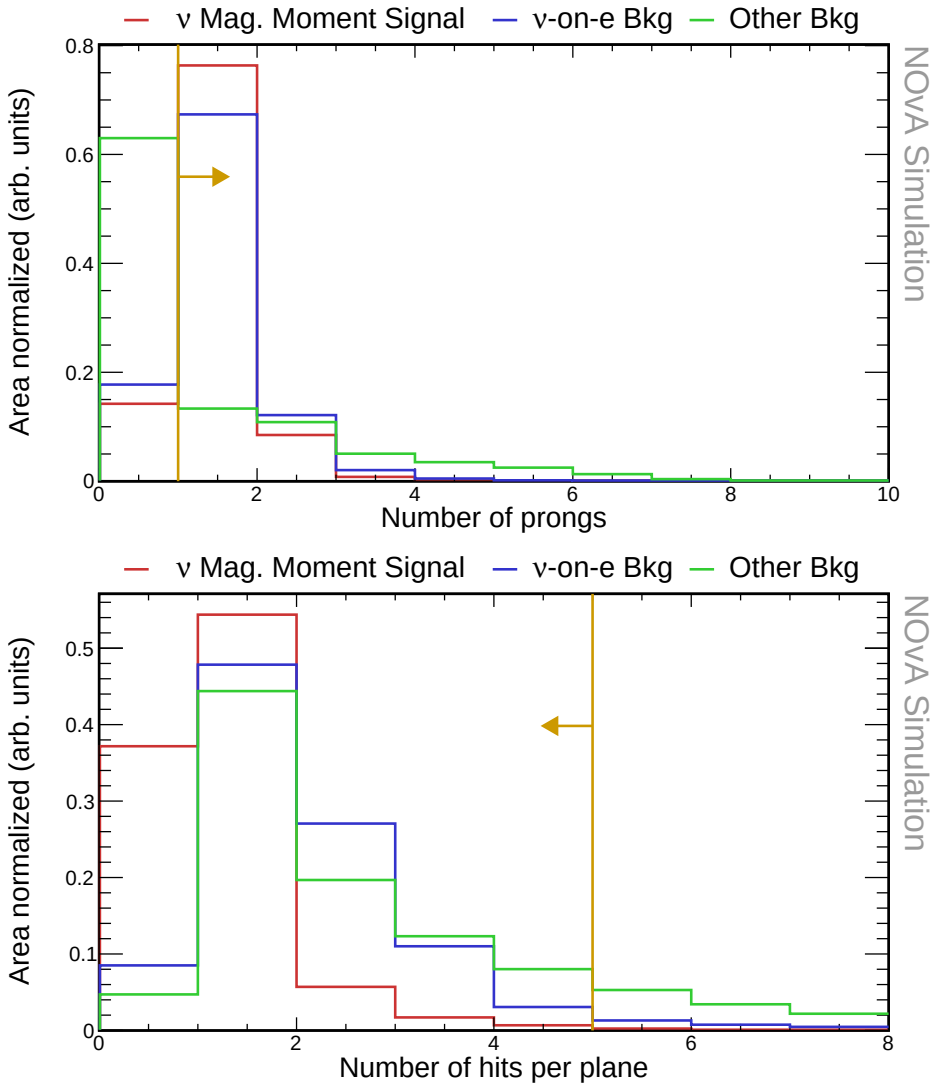

Figure 2.7: Relative comparison of signal (red), ν-on-e background (blue), and other background (green) events in the number of prongs (top) and the number of hits per plane (bottom) distributions. Events in both plots are required to have a valid reconstructed vertex and in the bottom plot also at least one reconstructed prong. Yellow lines indicate the cut values for the shown variables, with arrows pointing towards the preserved events. All histograms are area-normalised.

for lower energies - is this true though? - also there are further unexplored backgrounds that would need to be further studied and explore. Maybe depends on where would we move the cut...)

The reconstructed calorimetric energy of the primary shower is required to be $E_{cal} > 0.5\,\mathrm{GeV}$ as shown in Fig. 2.8. This is to remove region in the parameter space with large backgrounds. However, due to the nature of the neutrino magnetic moment signal, this cut also removes a majority of our signal events (exactly how much?).

This is due to a presence of large background that has not been studied very well. No NOvA analysis really uses events with such low energies. However, after further studies and validation, it is likely that these cut can be pushed to lower electron recoil energy, especially by using better event identifiers to remove the large background there.

NOvA is not super well suited for a low energy detection and there are troubles identifying very low energetic event. Majority of the analyses in NOvA only use events with energies above $0.5\,\mathrm{GeV}$. nueCCXSec only uses events above 1 GeV. The numuCCpi0 XSec ana had a low E cutoff at 0.1GeV

COMMENT: *How does the energy resolution and bias come into play here? 0.5GeV for us is not the same as for the 3fl or for some other ND analyses. This needs to be properly investigated in the future*

Maybe also say that Test Beam will be crucial in improving the vertex and energy resolution within NOvA, including electrons.

Table 2.4: Event selection cutflow table for the reconstruction quality cuts showing the number of events and the relative efficiency of each cut for each signal sample. The relative efficiency is calculated as number of events remaining after applying the corresponding cut divided by number of event for all the previous cuts. All the cuts are listed in sequence as they are applied.

Selection	**Signal**		**ν-on-e bkg**		**Other bkg**	
	N_{evt}	ϵ_{rel} (%)	N_{evt}	ϵ_{rel} (%)	N_{evt}	ϵ_{rel} (%)
No Cut	269.77	100	3.43×10^{3}	100	2.96×10^{8}	100
Valid Vtx	180.58	66.94	3.33×10^{3}	96.94	2.34×10^{8}	79.10
N^o Prongs	174.69	96.74	3.23×10^{3}	96.99	8.66×10^{7}	37.00
Hits / Plane	174.36	99.81	3.22×10^{3}	93.83	7.32×10^{7}	84.55
Low E_{Shower}	48.75	27.96	2.71×10^{3}	84.10	4.06×10^{7}	55.52

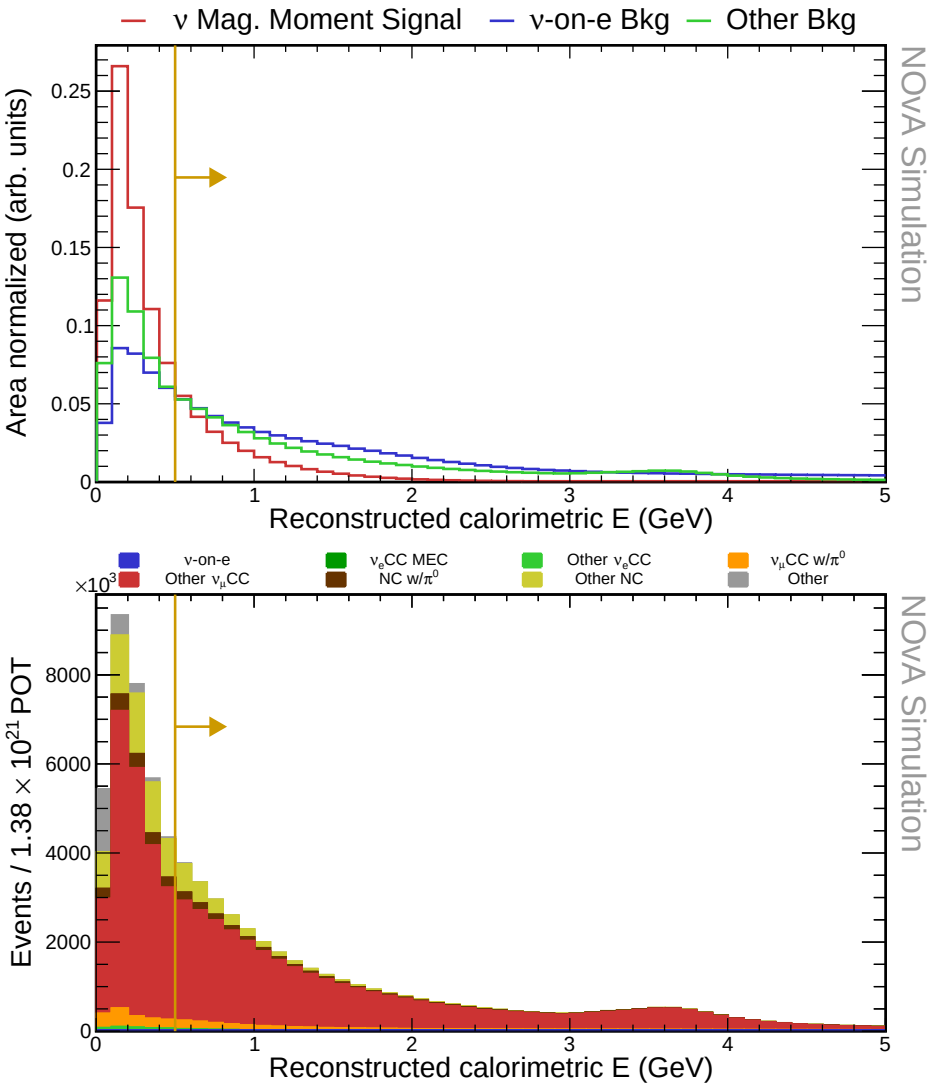

Figure 2.8: Top: Relative comparison of signal (red), ν-on-e background (blue), and other background (green) events in the reconstructed calorimetric energy distribution. All histograms are area-normalised. Bottom: Decomposition of background into various sub-samples, normalised to the data POT exposure. Events in both plots are required to have a valid reconstructed vertex, at least one reconstructed prong and at most 5 hits per plane. Yellow lines indicate the cut value for the reconstructed calorimetric energy, with arrows pointing towards the preserved events.

2.3.3 Basic Event Selection

Basic event selection cuts aim to remove obvious background events without affecting the signal too much. The criterion for these cuts will be that each of them has to limit the signal efficiency by approximately $0.25\,\%$. This means that in total the pre-selection cuts will lower the signal efficiency by only approximately $1\,\%$. We are using the same variables for these cuts as were used in the event selection for the ν_e appearance ND constraint for the three flavour neutrino oscillation measurements [54]. Additionally, we are also using a cut on the product of the reconstructed calorimetric energy and the square of the reconstructed angle between the recoil electron and the neutrino beam direction. The electron is assumed to be the most energetic reconstructed showers. The reconstructed showers are ordered based on their deposited energies, therefore the first reconstructed prong is assumed to be the most energetic. In case of the ν-on-e events, this should be the electron.

They also remove the obvious ν_μCC interactions by requiring that the summed number of cells for all prongs in the slice is < 200 and the length of the longest prong is < 540 cm. Relative comparison of signal, ν-on-e background, and other background distributions for the pre-selection variables is shown on Fig. **??**.

Additionally, as discussed in Sec. 2.1.2, from theory we know what the true recoil electron for the ν-on-e interaction is supposed to be limited by $E\theta^2 < 2m_e$. Due to reconstruction deficiencies, the reconstructed $E\theta^2$ will not have such a strict cut-off for ν-on-e events, this variable can however be used to distinguish them from the ν_eCC events, for which the electron has a much more isotropic distribution.

On top of that, we are also placing a loose cut on the maximum calorimetric energy, as the signal is limited to low energies, as can be seen in Fig. 2.11.

Some of the signal events can be reconstructed with the opposite direction than the beam. These events might still be useful though and we want to keep them. For that reason, we are calculating the angle between the outgoing electron and the neutrino beam direction as $\mathrm{acos}\,(\mathrm{abs}\,(\cos\theta))$, which gives the same value whether the shower is reconstructed forward or backwards.

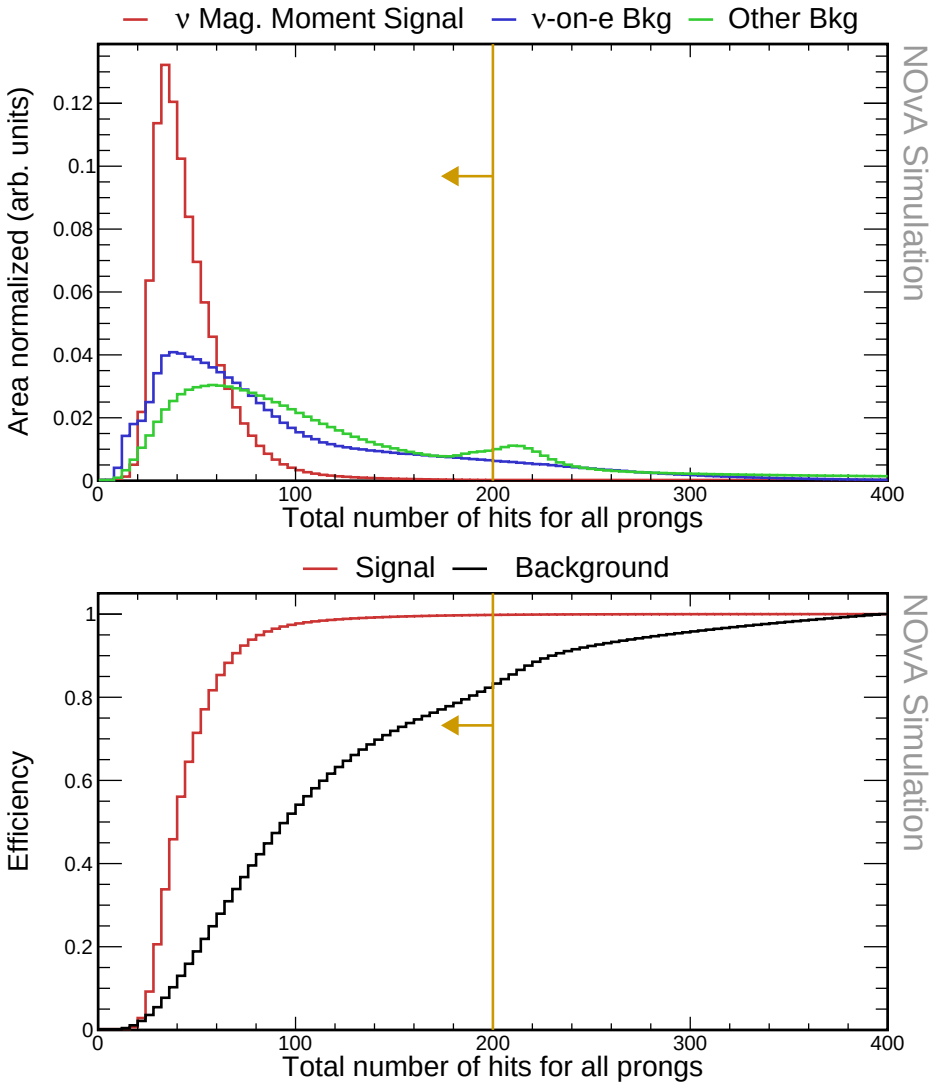

Figure 2.9: Top: Relative comparison of signal (red), ν-on-e background (blue), and other background (green) events in the distribution of total number of hits from all reconstructed prongs in the slice. All histograms are area-normalised. Bottom: Cumulative signal (red) and background (black) efficiency calculated as number of signal/background events left of the bin divided by the total number of signal/background events. Yellow lines indicate the cut value for the maximum number of hits, with arrows pointing towards the preserved events. The reconstruction quality cuts were applied before making these plots.

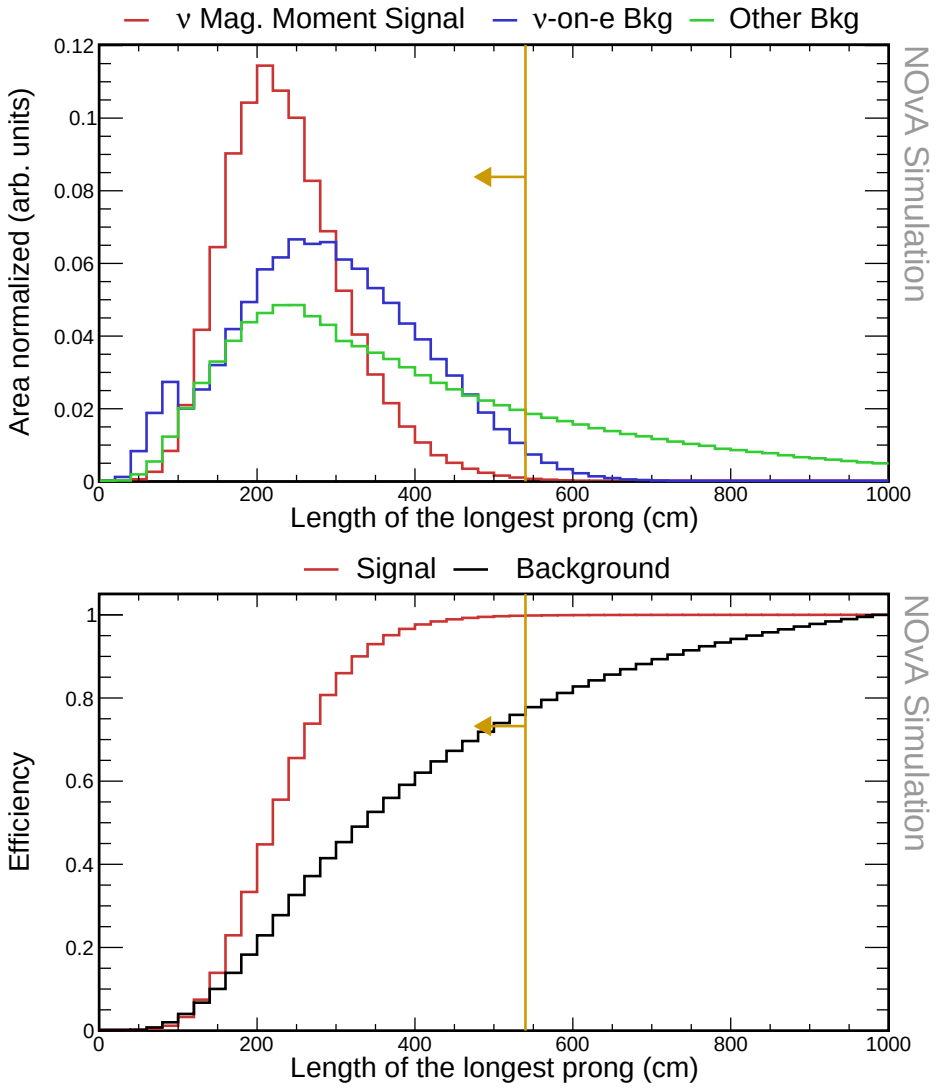

Figure 2.10: Top: Relative comparison of signal (red), ν-on-e background (blue), and other background (green) events in the distribution of the length of the longest reconstructed prong in slice. All histograms are area-normalised. Bottom: Cumulative signal (red) and background (black) efficiency calculated as number of signal/background events left of the bin divided by the total number of signal/background events. Yellow lines indicate the cut value for the maximum length of the longest prong, with arrows pointing towards the preserved events. The reconstruction quality cuts and the number of hits cut were applied before making these plots.

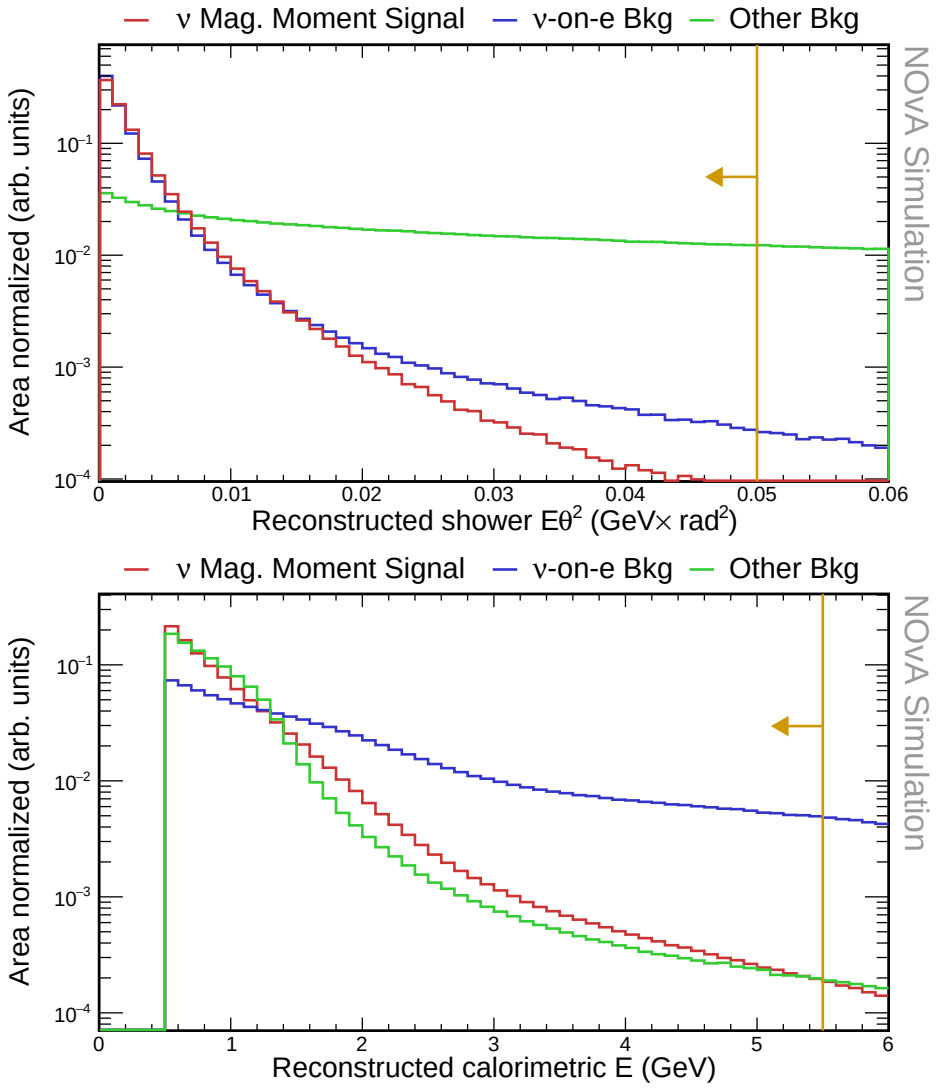

Figure 2.11: Relative comparison of signal (red), ν-on-e background (blue), and other background (green) events in the distribution of the reconstructed energy of the leading shower multiplied by its angle from the incoming neutrino beam direction squared (top) and of the reconstructed energy of the leading shower (bottom). All histograms are area-normalised with logarithmic y axis. Yellow lines indicate the cut value for the corresponding variables, with arrows pointing towards the preserved events. The reconstruction quality cuts, the number of hits cut, and the length of the longest prong cuts were applied before making both of these plots, while the hits in the bottom plot are also required to pass the $E\theta^2$ cut.

2.3.4 Fiducial and containment cuts

[nueXSec ana, docdb:37668] For both the X and Y vertices the distributions are asymmetric when comparing across the origin, in terms of vertex position. This is primarily due to particles coming from the +y and -x from events in the rock surrounding the detector. This corresponds to the direction of the NuMI target from the near detector. ...We require all activity from neutrino activity be deposited outside of the muon catcher.

TO DO: *Describe what does the fiducial cut do* We require that the reconstructed vertex is contained within the following volume: $-175 < \mathrm{Vtx}_X < 175, -175 < \mathrm{Vtx}_Y < 175, 95 < \mathrm{Vtx}_Z < 1095$ cm.

To ensure all the energy is contained within the detector and to remove events originating outside of the detector (rock muons), we require that the extreme positions of hits for all prongs in the slice are within the following volume: $-175 < \mathrm{min}_X, \mathrm{max}_X < 175, -175 < \mathrm{min}_Y, \mathrm{max}_Y < 175, 105 < \mathrm{min}_Z, \mathrm{max}_Z < 1270$ cm. COMMENT: *Also made this a bit stricter from the ND group's values as it didn't really make sense*

2.3.5 Event Selection Optimization

COMMENT: *This is where I started the TMVA*

Table 2.5: Basic event selection cutflow table showing the number of events and the relative efficiency of each cut for each signal sample. The relative efficiency is calculated as number of events remaining after applying the corresponding cut divided by number of event for all the previous cuts. All the cuts are listed in sequence as they are applied. The top row corresponds to the sample after applying the reconstruction quality cuts.

Selection	**Signal**		**ν-on-e bkg**		**Other bkg**	
	N_{evt}	ϵ_{rel} (%)	N_{evt}	ϵ_{rel} (%)	N_{evt}	ϵ_{rel} (%)
Reco Quality	48.75	100	2.71×10^3	100	4.06×10^7	100
N^o Hits Loose	48.64	99.78	2.32×10^3	85.63	3.08×10^7	75.67
Prong Length	48.52	99.75	2.26×10^3	97.39	2.17×10^7	70.66
$E\theta^2$ **Loose**	48.39	99.73	2.25×10^3	99.71	6.00×10^6	27.62
High E_{Shower} **Loose**	48.27	99.76	2.03×10^3	90.04	5.98×10^6	99.67

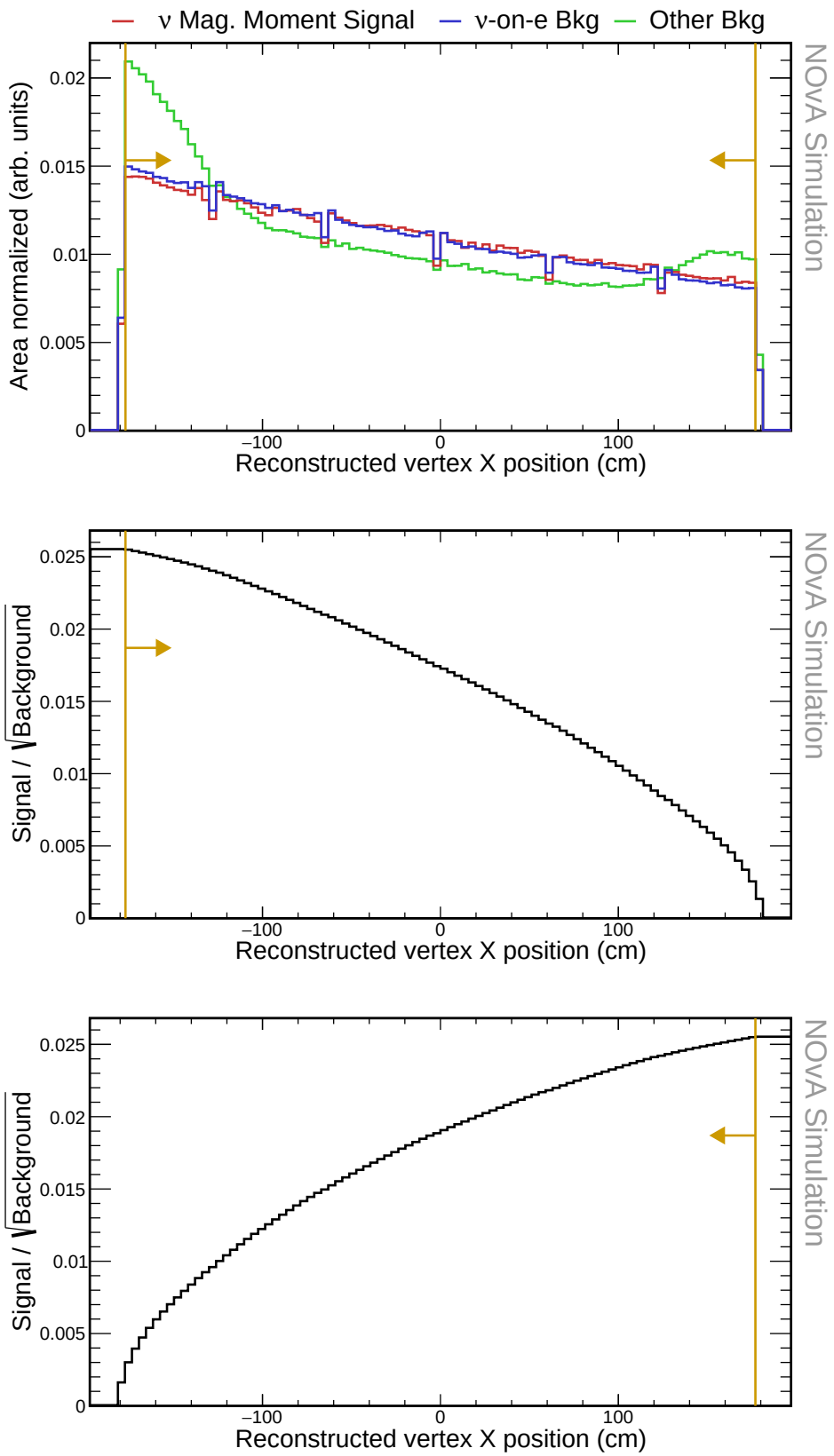

Figure 2.12: Top: Relative comparison of signal (red), ν-on-e background (blue), and other background (green) events in the distribution of the x position of the reconstructed vertex. All histograms are area-normalized. Middle and bottom: Cumulative FOM calculated as the number of signal events, divided by the number of background events from that bin until the end of the plot in the direction of the yellow arrow. The reconstruction quality and basic selection cuts were applied prior to making these plots. Additionally, vertex is required to be within the active region of the detector ($Vtx_Z < 1270\,\mathrm{cm}$). Yellow lines show the cut values that create the fiducial volume, with arrows pointing towards the preserved events.

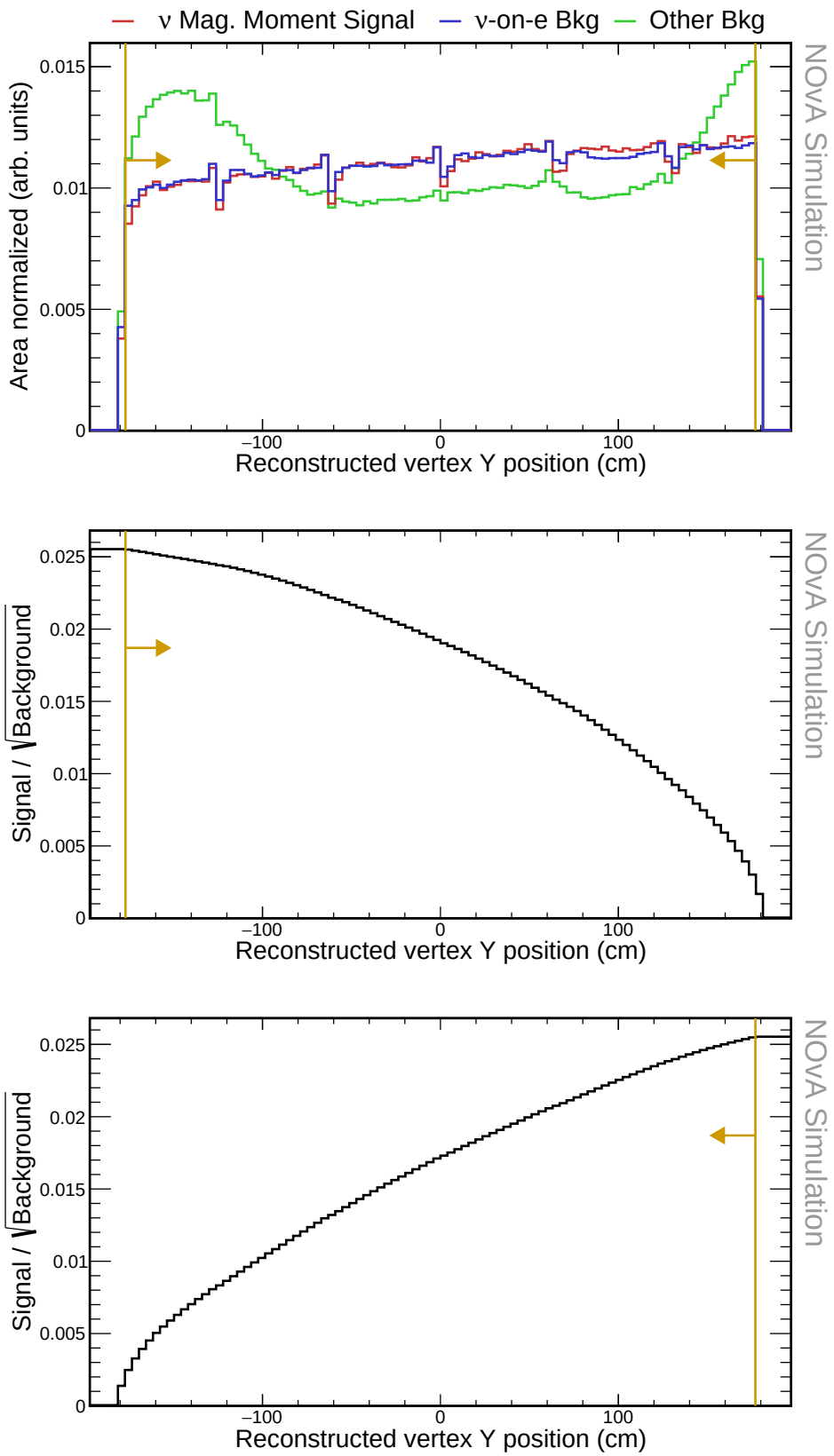

Figure 2.13: Top: Relative comparison of signal (red), ν-on-e background (blue), and other background (green) events in the distribution of the y position of the reconstructed vertex. All histograms are area-normalized. Middle and bottom: Cumulative FOM calculated as the number of signal events, divided by the number of background events from that bin until the end of the plot in the direction of the yellow arrow. The reconstruction quality and basic selection cuts were applied prior to making these plots. Additionally, vertex is required to be within the active region of the detector ($Vtx_Z < 1270\,\mathrm{cm}$). Yellow lines show the cut values that create the fiducial volume, with arrows pointing towards the preserved events.

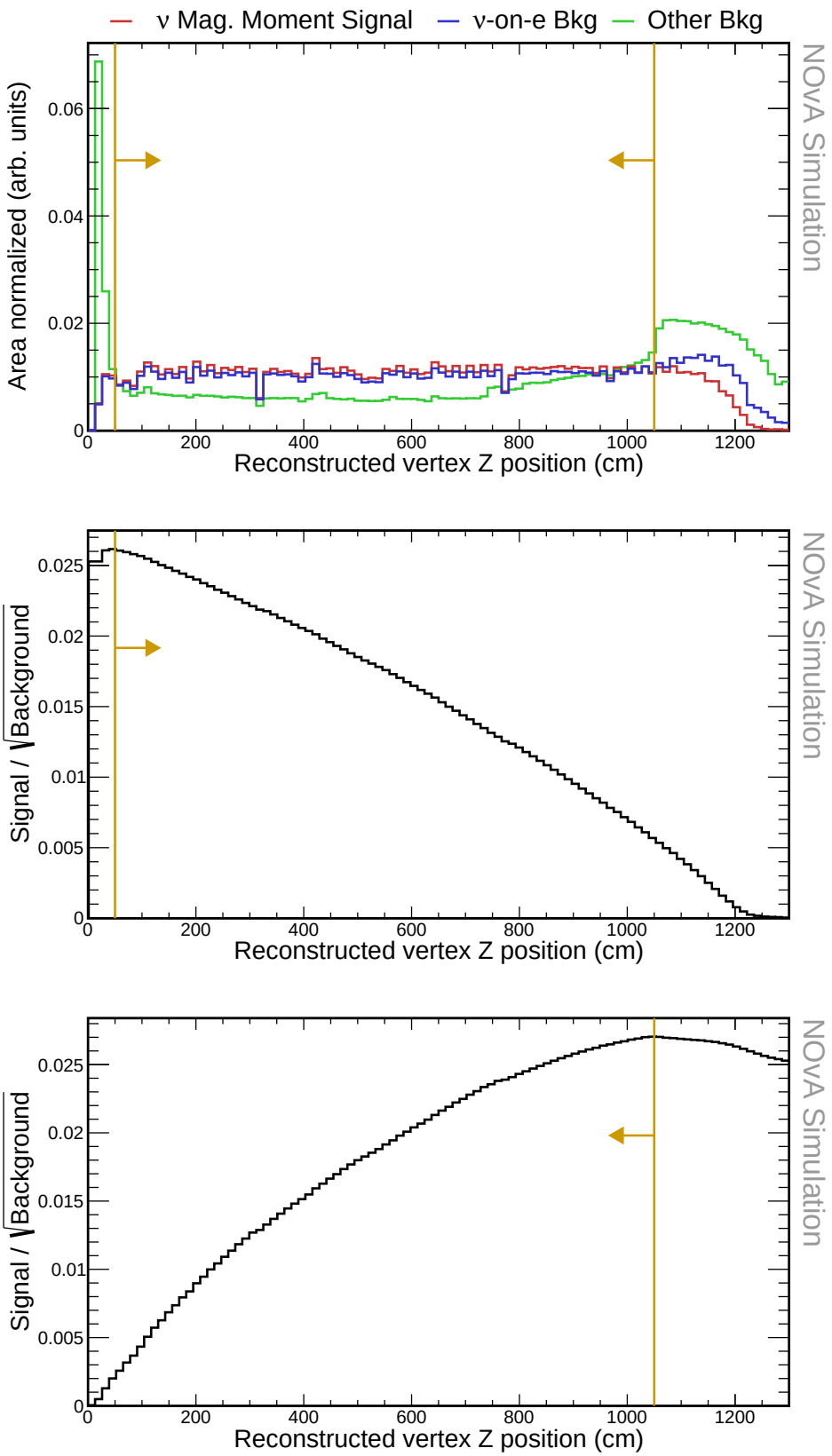

Figure 2.14: Top: Relative comparison of signal (red), ν-on-e background (blue), and other background (green) events in the distribution of the z position of the reconstructed vertex. All histograms are area-normalized. Middle and bottom: Cumulative FOM calculated as the number of signal events, divided by the number of background events from that bin until the end of the plot in the direction of the yellow arrow. The reconstruction quality and basic selection cuts were applied prior to making these plots. Yellow lines show the cut values that create the fiducial volume, with arrows pointing towards the preserved events.

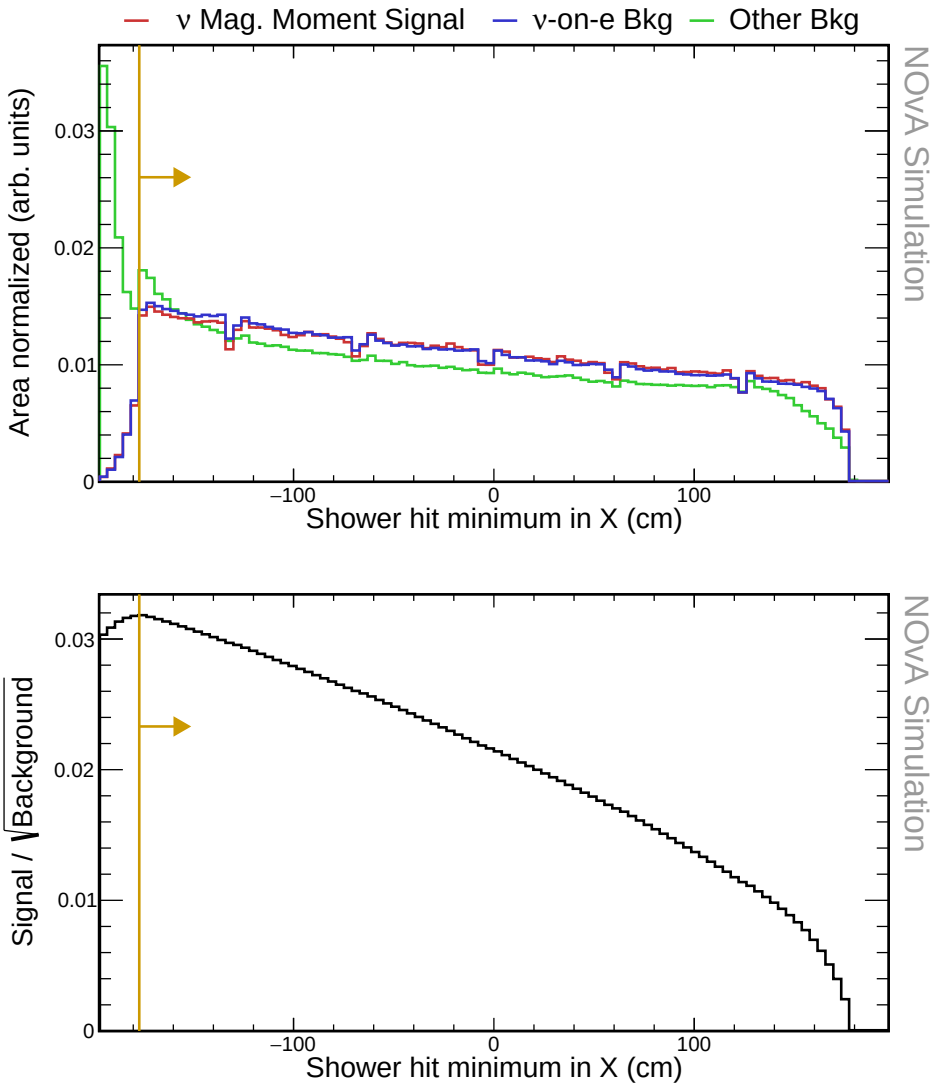

Figure 2.15: Relative comparison of signal, ν-on-e background, and other background events for the minimum and maximum position of the reconstructed shower along the x axis. Pre-selection and fiducial cuts were applied to make these plots. Gold lines show the values of the containment cuts.

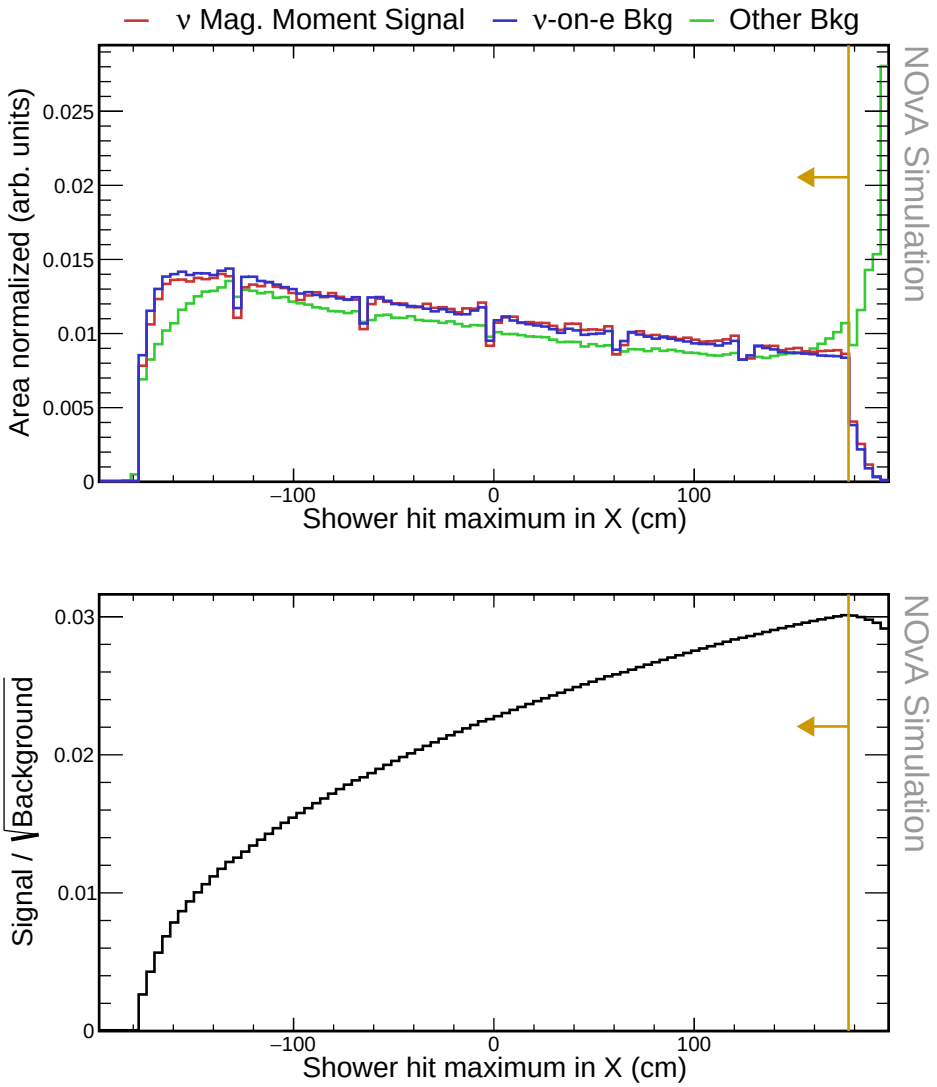

Figure 2.16: Relative comparison of signal, ν-on-e background, and other background events for the minimum and maximum position of the reconstructed shower along the x axis. Pre-selection and fiducial cuts were applied to make these plots. Gold lines show the values of the containment cuts.

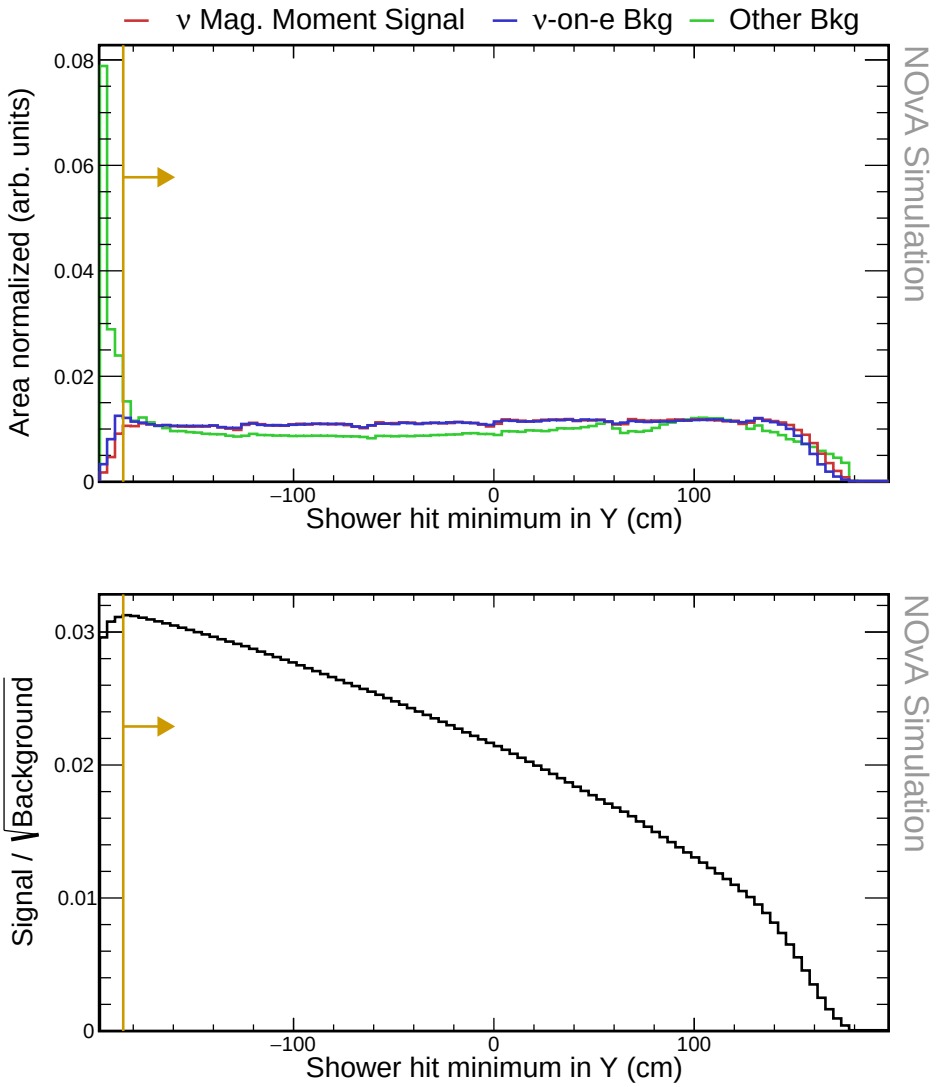

Figure 2.17: Relative comparison of signal, ν-on-e background, and other background events for the minimum and maximum position of the reconstructed shower along the y axis. Pre-selection and fiducial cuts were applied to make these plots. Gold lines show the values of the containment cuts.

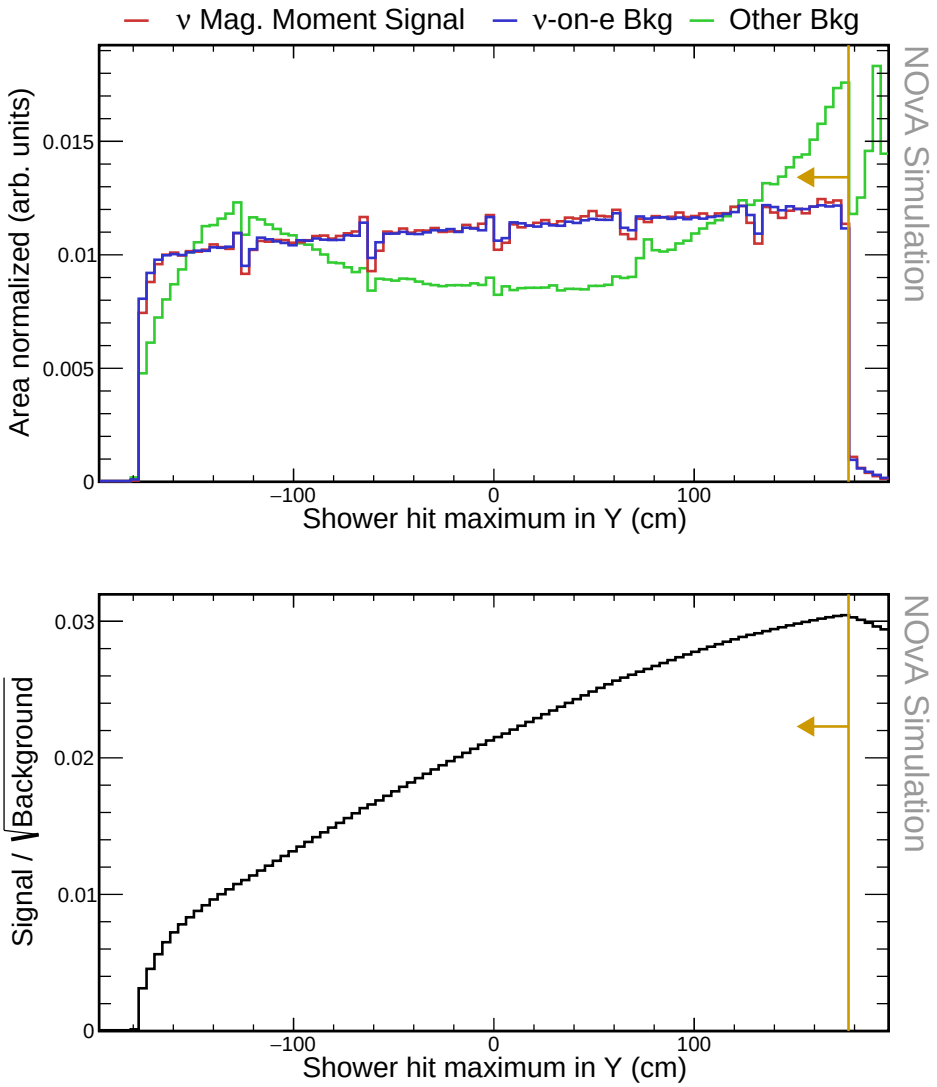

Figure 2.18: Relative comparison of signal, ν-on-e background, and other background events for the minimum and maximum position of the reconstructed shower along the y axis. Pre-selection and fiducial cuts were applied to make these plots. Gold lines show the values of the containment cuts.

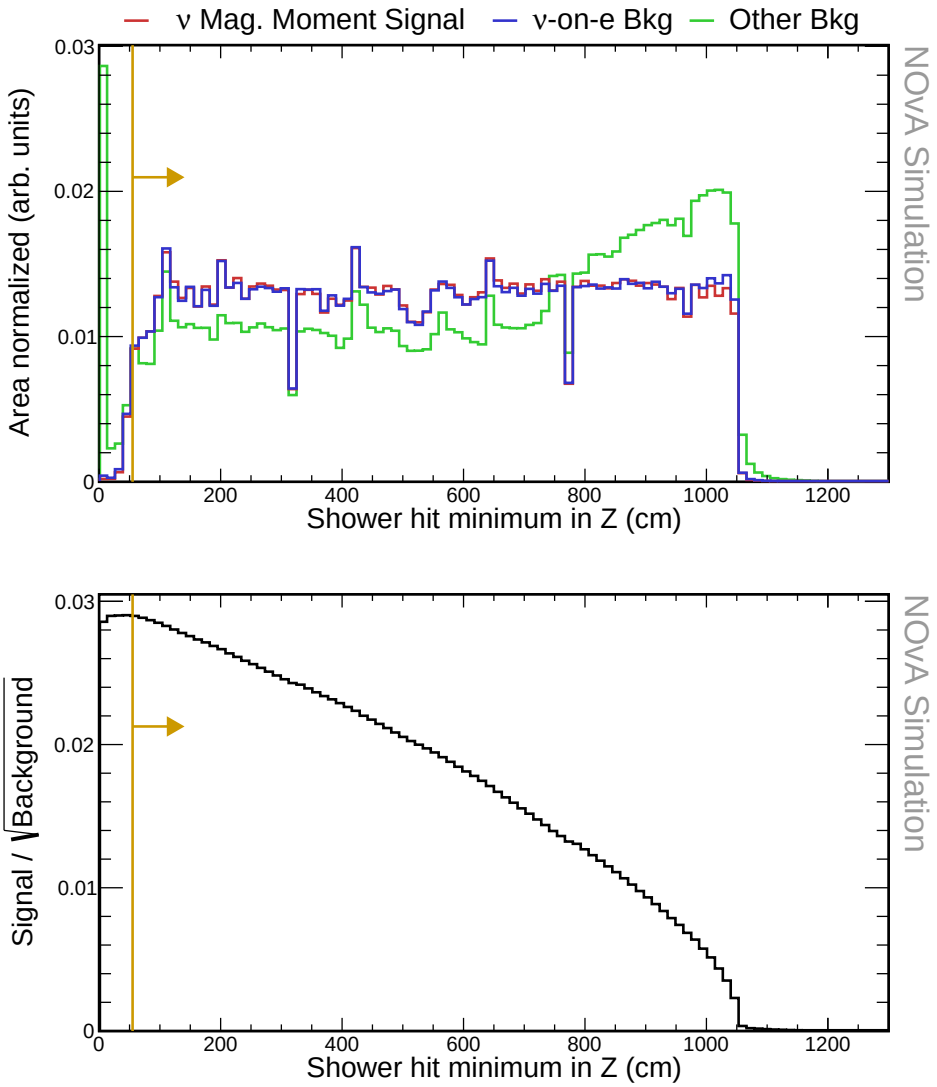

Figure 2.19: Relative comparison of signal, ν-on-e background, and other background events for the minimum and maximum position of the reconstructed shower along the z axis. Pre-selection and fiducial cuts were applied to make these plots. Gold lines show the values of the containment cuts.

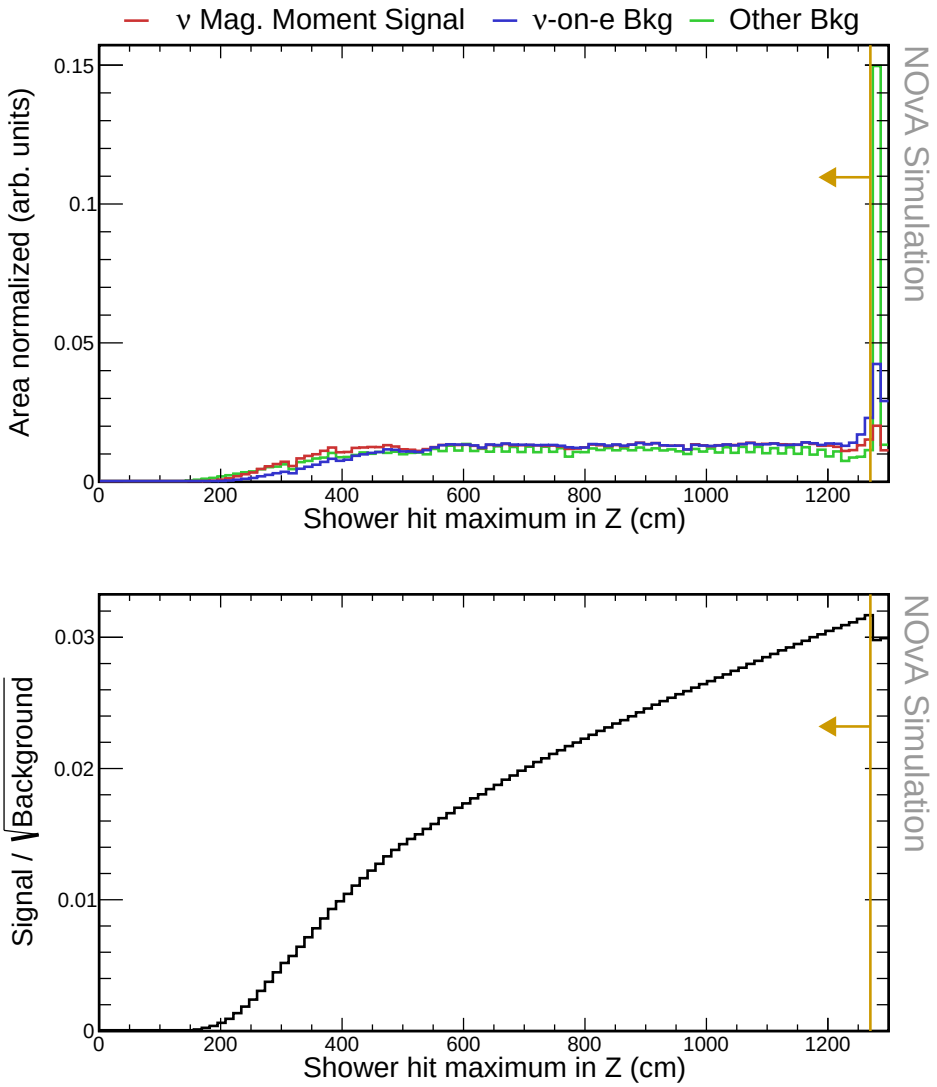

Figure 2.20: Relative comparison of signal, ν-on-e background, and other background events for the minimum and maximum position of the reconstructed shower along the z axis. Pre-selection and fiducial cuts were applied to make these plots. Gold lines show the values of the containment cuts.

Single Shower Requirement

To selection events with a single particle we require that the fraction of energy contained in the most energetic shower is > 0.8, that the summed energy of all cells (above threshold and within ± 8 planes from the vertex) outside of the most energetic shower is < 0.02 GeV, and that the distance between the vertex and the start of the primary shower is < 20 cm.

Event Classifiers

We are using two event classifiers based on convolution neural network that were developed specifically to identify ν-on-e interactions. The first one (`NuoneID`) is trained to select ν-on-e events and the second one (`Epi0ID`) is trained on the events passing the `NuoneID` to reject the π^0 background. Our selection requires that `NuoneID`> 0.73 and that `Epi0ID`> 0.92.

TO DO: *reference theory for the kinematics of nuone scattering* We require that the product of reconstructed energy of the primary shower and the square of its angle from the Z axis is $E_{cal}\theta^2 < 0.005$ GeV $\times$ rad^2.

TO DO: *Add plots of distributions of the event selection variables with two columns. LHS shows no cuts applied and RHS shows all previous cuts applied*

Using the many plots below that show the effect of each of the cuts on the signal and all background events. (For signal we are showing NuMM=...)

[ND group's technote] Two event classifiers (NuoneID and Epi0ID) based on convolutional neural network (CNN) are trained to identify nuone elastic scattering events (NuoneID) and to further reject background with pi0 in the final state (Epi0ID). The CNN architecture adopted for this analysis is the one used for NOvA CVN [12]. It

Table 2.6: Event selection cutflow table for the reconstruction quality cuts showing the number of events and the relative efficiency of each cut for each signal sample. The relative efficiency is calculated as number of events remaining after applying the corresponding cut divided by number of event for all the previous cuts. All the cuts are listed in sequence as they are applied.

Selection	**Signal**		**ν-on-e bkg**		**Other bkg**	
	N_{evt}	ϵ_{rel} (%)	N_{evt}	ϵ_{rel} (%)	N_{evt}	ϵ_{rel} (%)
Basic selection	48.27	100	2.03×10^3	100	5.98×10^6	100
Fiducial	45.51	94.27	1.89×10^3	93.36	2.89×10^6	48.22
Containment	42.01	92.31	1.62×10^3	85.42	7.22×10^5	25.04

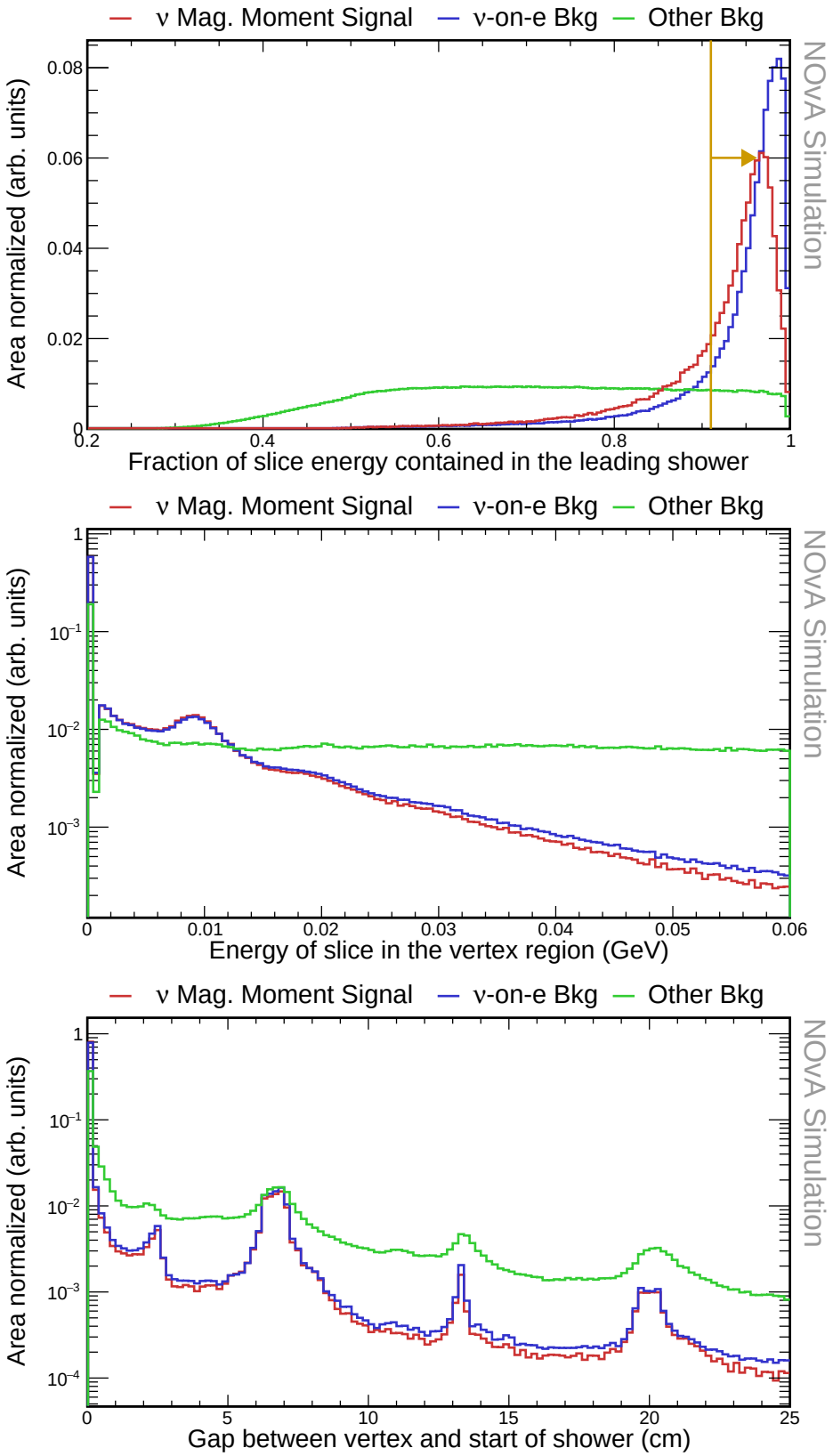

Figure 2.21: TMVA variables before the TMVA results. Relative comparison of signal, ν-on-e background, and other background events for the reconstructed vertex. Every previous cut was applied to make these plots, including the ShwECont for the middle and the bottom plot and the VtxE cut for the bottom plot. Gold lines show the cut values that create the fiducial volume.

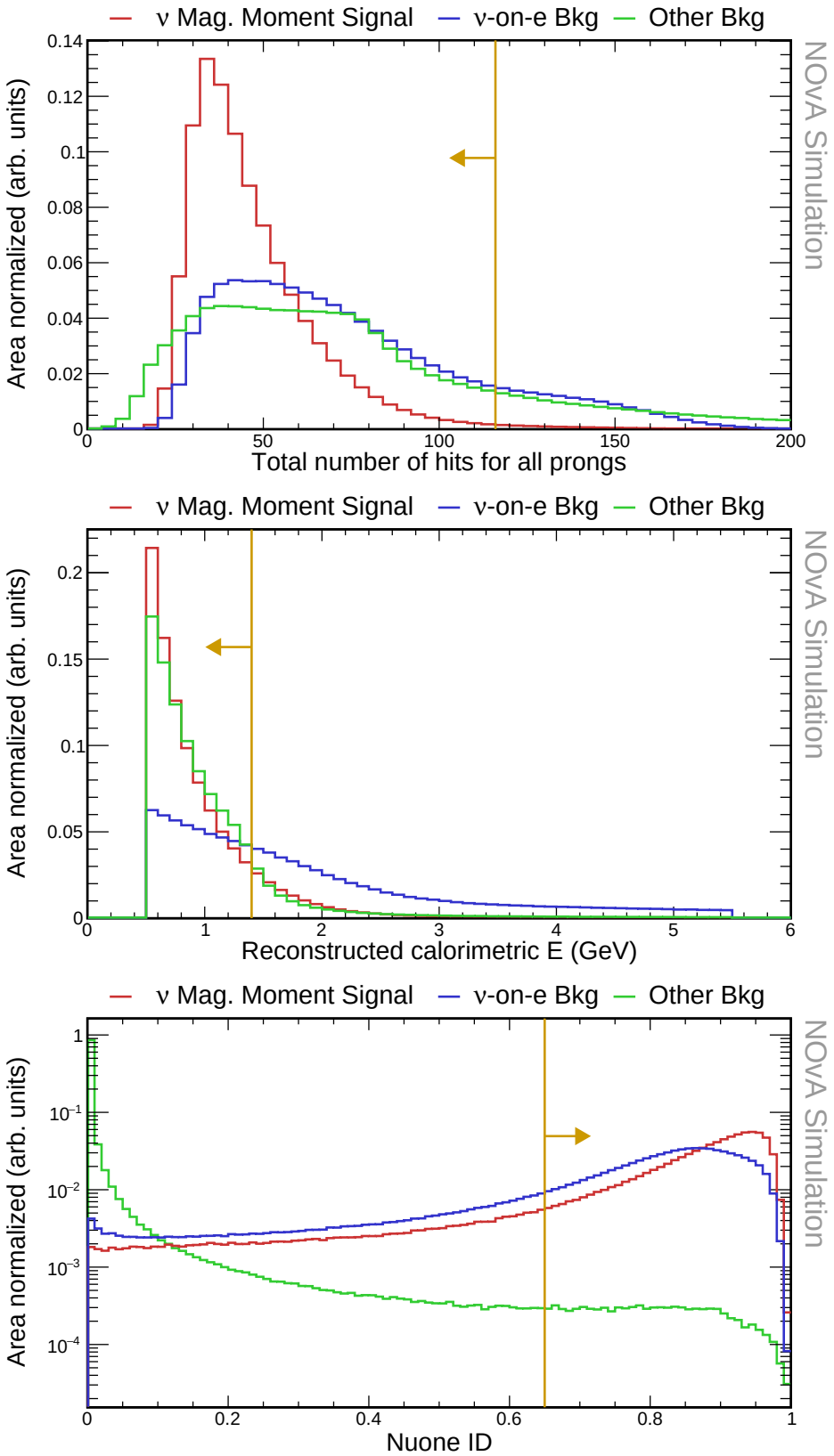

Figure 2.22: Relative comparison of signal, ν-on-e background, and other background events for the reconstructed vertex. No cuts were applied to make these plots. All the previous cuts were applied, including the cut on the shower energy. No single particle or event ID cuts were applied yet though. Gold lines show the cut values that create the fiducial volume.

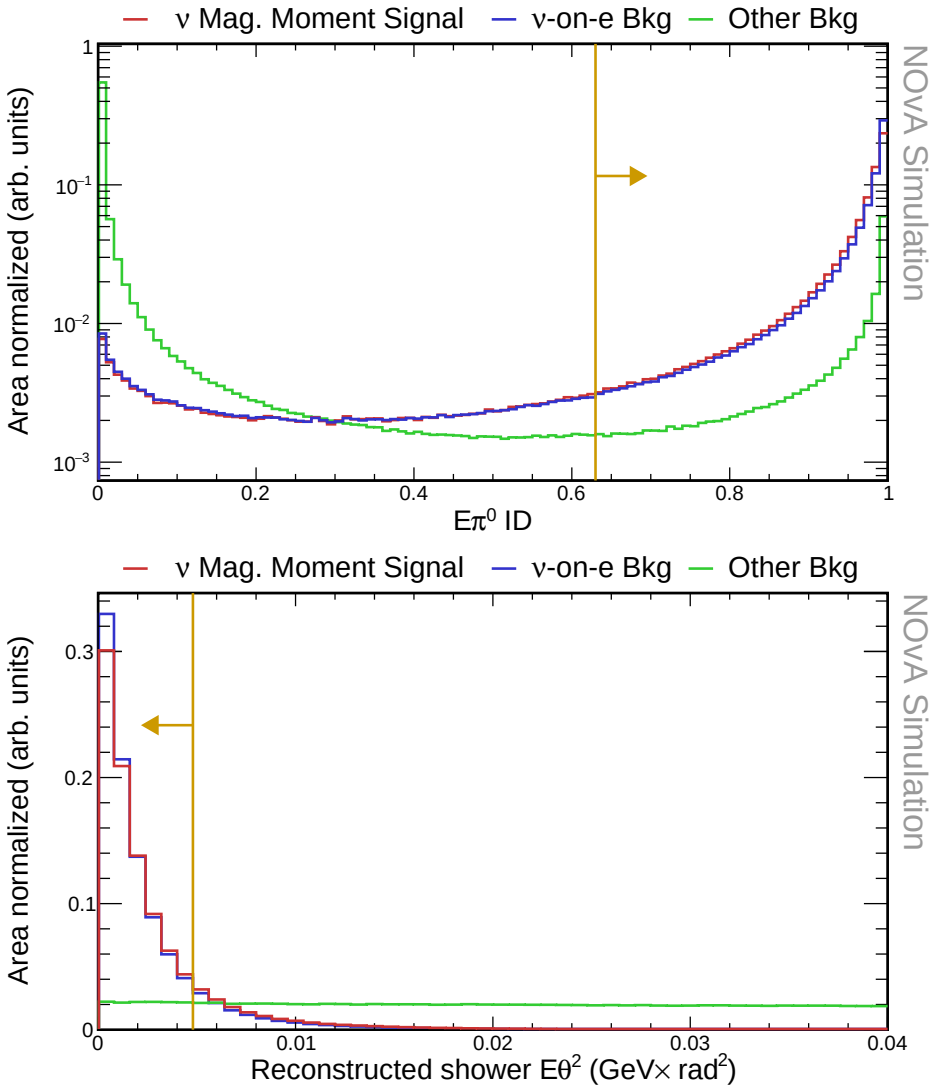

Figure 2.23: Relative comparison of signal, ν-on-e background, and other background events for the reconstructed vertex. No cuts were applied to make these plots. All the previous cuts were applied, including the cut on the shower energy. No single particle or event ID cuts were applied yet though. Gold lines show the cut values that create the fiducial volume.

takes the pixel map of a slice as the input and has deeper and more complicated neural networks than the ANNs used in the previous round of analysis [11]. The training for both classifiers (NuoneID and Epi0ID) were done with single electron samples as the signal in order to mitigate the model dependence. A nuone elastic scattering has an electron in the final state which could deposit energy in the detector. Single electron events share this feature with nuone elastic scattering, but have more uniform distribution of energy, angle between the shower direction and the beam direction. This additional feature could prevent CNN models from overfitting the feature of the very small scattering angle. To make comparisons, test samples of signal and background are normalized to 1.1E21. The output categories are ν-on-e, π^0, ν_eCC and other. The ν-on-e and π^0 outputs are used for the training of the Epi0ID. The pre-selection applied is: ND group's preselection ($L < 800\,\mathrm{cm}$, $N_{plane} < 120$, $N_{cell} < 600$), loose containment ($-190 < X < 190$, $-190 < Y < 190$, $50 < Z < 1500$ cm), loose single particle cut ($E_{vtx} < 0.05\,\mathrm{GeV}$, $gap < 20\,\mathrm{cm}$, $E_{shower}/E_{tot} > 0.9$ COMMENT: *These are quite strict actually*. The training accuracy for NuoneID is about 85% and for Epi0ID is about 96%. After each round of training, the trained model is saved to make predictions on the test sample so we know how the actual performance of the classifiers evolves over different epochs.

Multivariate Analysis

TMVA [88]

These event selection in total reduces signal $44.51\,\%$, ν-on-e background $70.40\,\%$ and other background $99.97\,\%$. After the full event selection, the predicted number of signal events for $\mu_\nu = 10^{-9}\mu_B$ is 23.31 and the total number of background events under the SM hypothesis is 678.26. The most likely improvement is in probing the low energetic events and making sure they make sense. Additionally, it is possible to use a specially designed control regions to mitigate the very high non-ν-on-e background.

TO DO: *Add a discussion of possible improvements on the event selection on its limitations - mostly for the analysis review committee* From here we can see that ... Maybe what can be improved is... This can likely be improved upon by specifically selection low energy events and removing the cut on the reconstructed shower energy.

2.4 Energy resolution and binning

TO DO: *Add the energy resolution and binning plots* Describe what events were used for the energy resolution study and how it was performed

What are the results

Final plot

The electron energy and angle distributions and resolutions. Are we going to fit in E, Th, or ETh2? Is there something else?

Show plots of Reco V True for both energy and angle. (Should I show it with or without the energy cut?). Also show the resolution plots.

Maybe also mention that Test Beam will help with improving the dead materials correction and generally improving the bias and resolution of the reconstructed energy, which won't have to depend on the comparison to simulation

2.5 Systematic uncertainties

2.6 Statistical analysis

We are basically doing two separate things:

1. Testing a hypothesis that there is no magnetic moment present in the signal. Can we reject the null hypothesis given our data?

Table 2.7: Event selection cutflow table for the reconstruction quality cuts showing the number of events and the relative efficiency of each cut for each signal sample. The relative efficiency is calculated as number of events remaining after applying the corresponding cut divided by number of event for all the previous cuts. All the cuts are listed in sequence as they are applied.

Selection	**Signal**		**ν-on-e bkg**		**Other bkg**	
	N_{evt}	ϵ_{rel} (%)	N_{evt}	ϵ_{rel} (%)	N_{evt}	ϵ_{rel} (%)
Pre-selection	42.01	100	1.62×10^3	100	7.22×10^5	100
E_{Shower}/E_{Tot}	40.32	95.98	1.57×10^3	96.87	2.79×10^5	38.60
N^o Hits	39.93	99.03	1.34×10^3	85.56	2.63×10^5	94.24
High E_{Shower}	34.70	86.91	714.28	53.28	2.22×10^5	84.58
ν-on-e ID	29.41	84.75	600.38	84.05	3.36×10^3	1.51
$E\pi^0$ **ID**	27.46	93.37	560.56	93.37	2.18×10^3	64.72
$E\theta^2$	23.31	84.88	478.83	85.42	199.42	9.17

2. If we can reject the null hypothesis we want to estimate the best fit of the parameter. Additionally, we want to put a limit (set a confidence interval) on the magnetic moment parameter.

What should be included here:

- Fit methodology: Detail the fitting techniques used to extract the muon neutrino magnetic moment from the data.
- Fit validation: Describe how the fit is validated, including any statistical tests used.
- Fake data studies: Explain the use of fake data or Monte Carlo simulations to test the robustness of the analysis.

2.7 Results

Show the money plot - full prediction in the binned energy distribution, including the full statistical and systematic uncertainties

Write out the total number of measured events and their corresponding uncertainties

Explain what are the results of the fit and the limits, discuss the statistical significance of the result

2.8 Discussion

What should be included here:

- Interpretation: Interpret the results in the context of the current understanding of neutrino physics.
- Implications: Explain the broader implications of your findings for the field of particle physics.
- Future work: Suggest directions for future research based on your results.

- Improvements in NOvA, more FHC data, including RHC data, better reconstruction, better simulation and calibration, better event selection, including sideband samples, more systematics studies, better fitting techniques...
- Future beyond NOvA - DUNE
  * What are the possibilities for DUNE?

2.9 Conclusion

Summarize the results and compare them to the introduction, including comparisons to other experiments and theory. Restate the significant of the measurement

Closing remarks

Acronyms

ν-on-e neutrino-on-electron. 13, 14, 16, 17, 21, 23, 25–31, 33, 34, 36–40, 42–45, 55, 56

2p2h two particle - two hole. 5, 6

APD Avalanche Photodiode. 32

BSM Beyond Standard Model. 10–15, 17, 18, 21

C.L. Confidence Level. 13, 14

CC Charged Current. 1, 2, 4–6, 8, 9, 23, 29, 30, 37, 55

CEvNS Coherent Elastic ν-Nucleus Scattering. 6

COHπ Coherent π (production). 6

CP Charge conjugation - Parity (symmetry). 1, 8, 10

CVN Convolutional Visual Network. 31

DCM Data Concentration Module. 32

DIS Deep Inelastic Scattering. 5

DUNE Deep Underground Neutrino Experiment. 10

FEB Front End Board. 32

FOM Figure Of Merit. 30, 42–44

FSI Final State Interaction. 6

HK Hyper-Kamiokande. 10

HNL Heavy Neutral Lepton. 12

LBL Long Baseline. 10

LDM Light Dark Matter. 14

MC Monte Carlo. 27

MEC Meson Exchange Current. 6, 29

ML Machine Learning. 32

MSW Mikheyev-Smirnov-Wolfenstein. 9

NC Neutral Current. 1–4, 6, 8, 9

ND Near Detector. 13, 14, 17, 20, 26, 27, 29, 30, 37

NOvA NuMI Off-axis ν_e Appearance (experiment). 10, 13, 14, 16, 17, 20, 23, 25–27, 29, 30, 32, 35

NP New Physics. 11, 18

PMNS Pontecorvo-Maki-Nakagawa-Sakata. 7, 8, 17, 19

POT Protons On Target. 27, 29, 31, 36

PPFX Package to Predict the Flux. 27

QE Quasi Elastic (interaction). 4–6

Res Resonant baryon production. 5

SK Super-Kamiokande. 9

SM Standard Model. 1, 2, 10–13, 15–18, 23, 25, 26, 30, 55

SNO Sudbury Neutrino Observatory. 9

T2K Tokai to Kamioka (experiment). 10

Bibliography

[1] Wolfgang Pauli. Pauli letter collection: letter to Lise Meitner. Typed copy. URL http://cds.cern.ch/record/83282.

[2] L. M. Brown. The idea of the neutrino. *Physics Today*, 31(9):23–28, September 1978. doi:10.1063/1.2995181. (Including translation of W. Pauli, Aufsdtze und Vortrdge u'ber Physik und Erkenntnistheorie, Braunschweig (1961)).

[3] H. A. Bethe. Ionization power of a neutrino with magnetic moment. *Mathematical Proceedings of the Cambridge Philosophical Society*, 31(1):108–115, 1935. doi:10.1017/S0305004100012998.

[4] Enrico Fermi. Tentativo di una teoria dei raggi β. *Il Nuovo Cimento (1924-1942)*, 11(1):1–19. ISSN 1827-6121. doi:10.1007/BF02959820.

[5] Fred L. Wilson. Fermi's theory of beta decay. *American Journal of Physics*, 36 (12):1150–1160, 1968. doi:10.1119/1.1974382. (A complete English translation of E.Fermi, Zeitschrift fur Physik 88, 161 (1934)).

[6] Sheldon L. Glashow. Partial-symmetries of weak interactions. *Nuclear Physics*, 22(4):579–588. ISSN 0029-5582. doi:10.1016/0029-5582(61)90469-2. URL https://www.sciencedirect.com/science/article/pii/0029558261904692.

[7] Steven Weinberg. A model of leptons. *Phys. Rev. Lett.*, 19:1264–1266, Nov 1967. doi:10.1103/PhysRevLett.19.1264.

[8] Abdus Salam. *Weak and electromagnetic interactions*, pages 244–254. doi:10.1142/9789812795915_0034.

[9] L. Landau. On the conservation laws for weak interactions. *Nuclear Physics*, 3(1):127–131. ISSN 0029-5582. doi:10.1016/0029-5582(57)90061-5. URL https://www.sciencedirect.com/science/article/pii/0029558257900615.

[10] T. D. Lee and C. N. Yang. Parity nonconservation and a two-component theory of the neutrino. *Phys. Rev.*, 105:1671–1675, Mar 1957. doi:10.1103/PhysRev.105.1671.

[11] Abdus Salam. On parity conservation and neutrino mass. *Nuovo Cim.*, 5:299–301, 1957. doi:10.1007/BF02812841.

[12] Peter W. Higgs. Broken symmetries and the masses of gauge bosons. *Phys. Rev. Lett.*, 13:508–509, Oct 1964. doi:10.1103/PhysRevLett.13.508.

[13] F. Englert and R. Brout. Broken symmetry and the mass of gauge vector mesons. *Phys. Rev. Lett.*, 13:321–323, Aug 1964. doi:10.1103/PhysRevLett.13.321.

[14] G. S. Guralnik, C. R. Hagen, and T. W. B. Kibble. Global conservation laws and massless particles. *Phys. Rev. Lett.*, 13:585–587, Nov 1964. doi:10.1103/PhysRevLett.13.585.

[15] Steven Weinberg. A model of leptons. *Phys. Rev. Lett.*, 19:1264–1266, Nov 1967. doi:10.1103/PhysRevLett.19.1264.

[16] Carlo Giunti and Chung W. Kim. *Fundamentals of Neutrino Physics and Astrophysics*. 2007. ISBN 978-0-19-850871-7.

[17] F. Reines and C. L. Cowan. Detection of the free neutrino. *Phys. Rev.*, 92:830–831, Nov 1953. doi:10.1103/PhysRev.92.830.

[18] Cowan Jr. C.L., Reines F., Harrison F.B., Kruse H.W., and McGuire A.D. Detection of the free neutrino: A confirmation. *Science*, 124(3212):103–104, July 1956. doi:10.1126/science.124.3212.103.

[19] F. Reines and C.L. Cowan. Neutrino physics. *Physics Today*, 10(8):12–18, 1957. doi:10.1063/1.3060455.

[20] B. Adeva et al. Measurement of Z^0 decays to hadrons and a precise determination of the number of neutrino species. *Phys. Lett. B*, 237:136–146, 1990. doi:10.1016/0370-2693(90)90476-M.

[21] S. Schael et al. Precision electroweak measurements on the Z resonance. *Phys. Rept.*, 427:257–454, 2006. doi:10.1016/j.physrep.2005.12.006.

[22] M. C. Goodman. Resource letter anp-1: Advances in neutrino physics. *American Journal of Physics*, 84:309–319, 2016. doi:10.1119/1.4962228.

[23] M. Schwartz. Feasibility of using high-energy neutrinos to study the weak interactions. *Phys. Rev. Lett.*, 4:306–307, Mar 1960. doi:10.1103/PhysRevLett.4.306.

[24] K. Kodama et al. Observation of tau neutrino interactions. *Phys. Lett. B*, 504: 218–224, 2001. doi:10.1016/S0370-2693(01)00307-0.

[25] K. Kodama et al. Final tau-neutrino results from the DONuT experiment. *Phys. Rev. D*, 78:052002, 2008. doi:10.1103/PhysRevD.78.052002.

[26] William J Marciano and Zohreh Parsa. Neutrino–electron scattering theory*. *Journal of Physics G: Nuclear and Particle Physics*, 29(11):2629. doi:10.1088/0954-3899/29/11/013.

[27] J. A. Formaggio and G. P. Zeller. From ev to eev: Neutrino cross sections across energy scales. *Rev. Mod. Phys.*, 84:1307–1341, Sep 2012. doi:10.1103/RevModPhys.84.1307.

[28] *Fundamental Physics at the Intensity Frontier*, 5 2012. doi:10.2172/1042577.

[29] D. Casper. The Nuance neutrino physics simulation, and the future. *Nucl. Phys. B Proc. Suppl.*, 112:161–170, 2002. doi:10.1016/S0920-5632(02)01756-5.

[30] Jr. Davis, Raymond, Don S. Harmer, and Kenneth C. Hoffman. Search for neutrinos from the sun. *Phys. Rev. Lett.*, 20:1205–1209, 1968. doi:10.1103/PhysRevLett.20.1205.

[31] G. Danby, J-M. Gaillard, K. Goulianos, L. M. Lederman, N. Mistry, M. Schwartz, and J. Steinberger. Observation of high-energy neutrino reactions and the existence of two kinds of neutrinos. *Phys. Rev. Lett.*, 9:36–44, Jul 1962. doi:10.1103/PhysRevLett.9.36.

[32] A. A. Aguilar-Arevalo et al. First measurement of the muon neutrino charged current quasielastic double differential cross section. *Phys. Rev. D*, 81:092005, May 2010. doi:10.1103/PhysRevD.81.092005.

[33] M. Sajjad Athar, A. Fatima, and S. K. Singh. Neutrinos and their interactions with matter. *Prog. Part. Nucl. Phys.*, 129:104019, 2023. doi:10.1016/j.ppnp.2022.104019.

[34] M. Martini, M. Ericson, G. Chanfray, and J. Marteau. Unified approach for nucleon knock-out and coherent and incoherent pion production in neutrino interactions with nuclei. *Phys. Rev. C*, 80:065501, Dec 2009. doi:10.1103/PhysRevC.80.065501.

[35] M. Martini, M. Ericson, G. Chanfray, and J. Marteau. Neutrino and antineutrino quasielastic interactions with nuclei. *Phys. Rev. C*, 81:045502, Apr 2010. doi:10.1103/PhysRevC.81.045502.

[36] M. Martini, M. Ericson, and G. Chanfray. Neutrino quasielastic interaction and nuclear dynamics. *Phys. Rev. C*, 84:055502, Nov 2011. doi:10.1103/PhysRevC.84.055502.

[37] D. Akimov et al. Observation of coherent elastic neutrino-nucleus scattering. *Science*, 357(6356):1123–1126. doi:10.1126/science.aao0990.

[38] B Pontecorvo. Mesonium and antimesonium. *Sov. Phys. JETP*, 33:549–551, 8 1957.

[39] B. Pontecorvo. Inverse beta processes and nonconservation of lepton charge. *Sov. Phys. JETP*, 7:172–173, 1958.

[40] Ziro Maki, Masami Nakagawa, and Shoichi Sakata. Remarks on the unified model of elementary particles. *Prog. Theor. Phys.*, 28:870–880, 1962. doi:10.1143/PTP.28.870.

[41] V. Gribov and B. Pontecorvo. Neutrino astronomy and lepton charge. *Physics Letters B*, 28(7):493–496. ISSN 0370-2693. doi:10.1016/0370-2693(69)90525-5. URL https://www.sciencedirect.com/science/article/pii/0370269369905255.

[42] M.C. Gonzalez-Garcia and Yosef Nir. Neutrino Masses and Mixing: Evidence and Implications. *Rev. Mod. Phys.*, 75:345–402, 2003. doi:10.1103/RevModPhys.75.345.

[43] L. Wolfenstein. Neutrino oscillations in matter. *Phys. Rev. D*, 17:2369–2374, May 1978. doi:10.1103/PhysRevD.17.2369.

[44] S.P. Mikheyev and A.Yu. Smirnov. Resonance Amplification of Oscillations in Matter and Spectroscopy of Solar Neutrinos. *Sov. J. Nucl. Phys.*, 42:913–917, 1985.

[45] M. Aglietta et al. Experimental study of atmospheric neutrino flux in the NUSEX experiment. *Europhysics Letters (EPL)*, 8(7):611–614, 04 1989. doi:10.1209/0295-5075/8/7/005.

[46] K. Daum et al. Determination of the atmospheric neutrino spectra with the Fréjus detector. *Zeitschrift für Physik C Particles and Fields*, 66(3):417–428, 1995. ISSN 1431-5858. doi:10.1007/BF01556368.

[47] R. Becker-Szendy et al. Electron- and muon-neutrino content of the atmospheric flux. *Phys. Rev. D*, 46:3720–3724, Nov 1992. doi:10.1103/PhysRevD.46.3720.

[48] Y. Fukuda et al. Atmospheric muon-neutrino / electron-neutrino ratio in the multiGeV energy range. *Phys. Lett. B*, 335:237–245, 1994. doi:10.1016/0370-2693(94)91420-6.

[49] Y. Fukuda et al. Evidence for oscillation of atmospheric neutrinos. *Phys. Rev. Lett.*, 81:1562–1567, 1998. doi:10.1103/PhysRevLett.81.1562.

[50] Q.R. Ahmad et al. Direct evidence for neutrino flavor transformation from neutral current interactions in the Sudbury Neutrino Observatory. *Phys. Rev. Lett.*, 89:011301, 2002. doi:10.1103/PhysRevLett.89.011301.

[51] Patrick Huber et al. Snowmass Neutrino Frontier Report. In *Snowmass 2021*, 11 2022.

[52] R. L. Workman and Others. Review of Particle Physics. *PTEP*, 2022:083C01, 2022. doi:10.1093/ptep/ptac097.

[53] Ivan Esteban, M. C. Gonzalez-Garcia, Michele Maltoni, Thomas Schwetz, and Albert Zhou. The fate of hints: updated global analysis of three-flavor neutrino oscillations. *JHEP*, 09:178, 2020. doi:10.1007/JHEP09(2020)178.

[54] M. A. Acero et al. Improved measurement of neutrino oscillation parameters by the NOvA experiment. *Phys. Rev. D*, 106(3):032004, 2022. doi:10.1103/PhysRevD.106.032004.

[55] K. Abe et al. Measurements of neutrino oscillation parameters from the T2K experiment using 3.6×10^{21} protons on target. *Eur. Phys. J. C*, 83(9):782, 2023. doi:10.1140/epjc/s10052-023-11819-x.

[56] B. Abi et al. Volume I. Introduction to DUNE. *Journal of Instrumentation*, 15(08): T08008. doi:10.1088/1748-0221/15/08/T08008.

[57] K. Abe et al. Hyper-Kamiokande Design Report. 5 2018.

[58] M. Aker et al. Direct neutrino-mass measurement with sub-electronvolt sensitivity. *Nature Phys.*, 18(2):160–166, 2022. doi:10.1038/s41567-021-01463-1.

[59] Aghanim, N. et al. Planck 2018 results - vi. cosmological parameters. *Astron. Astrophys.*, 641:A6. doi:10.1051/0004-6361/201833910.

[60] A. Aguilar et al. Evidence for neutrino oscillations from the observation of $\overline{\nu}_e$ appearance in a $\overline{\nu}_\mu$ beam. *Phys. Rev. D*, 64:112007, Nov 2001. doi:10.1103/PhysRevD.64.112007.

[61] A.A. Aguilar-Arevalo et al. Significant Excess of ElectronLike Events in the MiniBooNE Short-Baseline Neutrino Experiment. *Phys. Rev. Lett.*, 121(22):221801, 2018. doi:10.1103/PhysRevLett.121.221801.

[62] M.C. Gonzalez-Garcia and Michele Maltoni. Phenomenology with Massive Neutrinos. *Phys. Rept.*, 460:1–129, 2008. doi:10.1016/j.physrep.2007.12.004.

[63] Rabindra N. Mohapatra and Goran Senjanovic. Neutrino Mass and Spontaneous Parity Nonconservation. *Phys. Rev. Lett.*, 44:912, 1980. doi:10.1103/PhysRevLett.44.912.

[64] Ettore Majorana. Teoria simmetrica dell'elettrone e del positrone. *Nuovo Cim.*, 14:171–184, 1937. doi:10.1007/BF02961314. Translated by Luciano Maiani in"Soryushiron Kenkyu", 63 (1981) 149-462.

[65] E. Aprile et al. Excess electronic recoil events in XENON1T. *Phys. Rev. D*, 102: 072004, . doi:10.1103/PhysRevD.102.072004.

[66] E. Aprile et al. Search for New Physics in Electronic Recoil Data from XENONnT. *Phys. Rev. Lett.*, 129:161805, . doi:10.1103/PhysRevLett.129.161805.

[67] M. Atzori Corona, W. M. Bonivento, M. Cadeddu, N. Cargioli, and F. Dordei. New constraint on neutrino magnetic moment and neutrino millicharge from LUX-ZEPLIN dark matter search results. *Phys. Rev. D*, 107:053001. doi:10.1103/PhysRevD.107.053001.

[68] M. Agostini et al. Limiting neutrino magnetic moments with borexino phase-ii solar neutrino data. *Phys. Rev. D*, 96:091103. doi:10.1103/PhysRevD.96.091103.

[69] Amir N. Khan. Light new physics and neutrino electromagnetic interactions in XENONnT. *Physics Letters B*, 837:137650. ISSN 0370-2693. doi:10.1016/j.physletb.2022.137650. URL https://www.sciencedirect.com/science/article/pii/S0370269322007845.

[70] K. S. Babu, Sudip Jana, and Manfred Lindner. Large Neutrino Magnetic Moments in the Light of Recent Experiments. *JHEP*, 10:040. doi:10.1007/JHEP10(2020)040.

[71] L. B. Auerbach et al. Measurement of electron-neutrino electron elastic scattering. *Phys. Rev. D*, 63:112001. doi:10.1103/PhysRevD.63.112001.

[72] D. A. Krakauer et al. Limits on the neutrino magnetic moment from a measurement of neutrino - electron elastic scattering. 252:177–180. doi:10.1016/0370-2693(90)91100-P.

[73] L. A. Ahrens, S. H. Aronson, P. L. Connolly, B. G. Gibbard, M. J. Murtagh, S. J. Murtagh, S. Terada, D. H. White, J. L. Callas, D. Cutts, M. V. Diwan, J. S. Hoftun, B. W. Hughlock, R. E. Lanou, T. Shinkawa, Y. Kurihara, K. Amako, S. Kabe, Y. Nagashima, Y. Suzuki, S. Tatsumi, Y. Yamaguchi, K. Abe, E. W. Beier, D. C. Doughty, L. S. Durkin, S. M. Heagy, M. Hurley, A. K. Mann, F. M. Newcomer, H. H. Williams, T. York, D. Hedin, M. D. Marx, and E. Stern. Determination of electroweak parameters from the elastic scattering of muon neutrinos and antineutrinos on electrons. *Phys. Rev. D*, 41:3297–3316, Jun 1990. doi:10.1103/PhysRevD.41.3297.

[74] P. Vilain et al. Experimental study of electromagnetic properties of the muon-neutrino in neutrino - electron scattering. *Phys. Lett. B*, 345:115–118, 1995. doi:10.1016/0370-2693(94)01678-6.

[75] Biao Wang. *Muon-Neutrino Electron Elastic Scattering and a Search for the Muon-Neutrino Magnetic Moment in the NOvA Near Detector*. PhD thesis. URL https://scholar.smu.edu/hum_sci_physics_etds/1.

[76] Wenjie Wu and Yiwen Xiao. Constraint of the Integrated Neutrino Flux from Neutrino-Electron Elastic Scattering in the NOvA Near Detector. NOVA Document 56383. URL https://nova-docdb.fnal.gov/cgi-bin/sso/ShowDocument?docid=56383. NOvA technical note.

[77] Athula Wickremasinghe, Wenjie Wu, and Yiwen Xiao. Status of the Measurement of Neutrino-Electron Elastic Scattering in the NOvA Near Detector. In *Neutrino 2022*. URL https://indico.kps.or.kr/event/30/contributions/738/.

[78] Barnali Brahma, Tyler Horoho, and Mu Wei. TechNote: Light Dark Matter Search with NOvA Near Detector. NOVA Document 59439. URL https://nova-docdb.fnal.gov/cgi-bin/sso/ShowDocument?docid=59439. NOvA technical note.

[79] Carlo Giunti and Alexander Studenikin. Neutrino electromagnetic interactions: A window to new physics. *Rev. Mod. Phys.*, 87:531–591, Jun 2015. doi:10.1103/RevModPhys.87.531.

[80] Boris Kayser. Majorana neutrinos and their electromagnetic properties. *Phys. Rev. D*, 26:1662–1670, Oct 1982. doi:10.1103/PhysRevD.26.1662.

[81] José F. Nieves. Electromagnetic properties of majorana neutrinos. *Phys. Rev. D*, 26:3152–3158, Dec 1982. doi:10.1103/PhysRevD.26.3152.

[82] Carlo Giunti, Julieta Gruszko, Benjamin Jones, Lisa Kaufman, Diana Parno, and Andrea Pocar. Report of the Topical Group on Neutrino Properties for Snowmass 2021. 9 2022.

[83] Nicole F. Bell, Mikhail Gorchtein, Michael J. Ramsey-Musolf, Petr Vogel, and Peng Wang. Model independent bounds on magnetic moments of Majorana neutrinos. *Phys. Lett. B*, 642:377–383, 2006. doi:10.1016/j.physletb.2006.09.055.

[84] Nicole F. Bell, Vincenzo Cirigliano, Michael J. Ramsey-Musolf, Petr Vogel, and Mark B. Wise. How magnetic is the Dirac neutrino? *Phys. Rev. Lett.*, 95:151802, 2005. doi:10.1103/PhysRevLett.95.151802.

[85] E. Valencia, D. Jena, Nuruzzaman, F. Akbar, L. Aliaga, D. A. Andrade, M. V. Ascencio, A. Bashyal, L. Bellantoni, A. Bercellie, A. Bodek, J. L. Bonilla, A. Bravar, H. Budd, G. Caceres, T. Cai, M. F. Carneiro, J. Chaves, D. Coplowe, H. da Motta, S. A. Dytman, G. A. Díaz, J. Felix, L. Fields, A. Filkins, R. Fine, N. Fiza, A. M. Gago, R. Galindo, H. Gallagher, A. Ghosh, T. Golan, R. Gran, D. A. Harris, S. Henry, S. Jena, J. Kleykamp, M. Kordosky, D. Last, T. Le, X.-G. Lu, E. Maher, S. Manly, W. A. Mann, C. Mauger, K. S. McFarland, A. M. McGowan, B. Messerly, J. Miller, J. G. Morfín, D. Naples, J. K. Nelson, C. Nguyen, A. Norrick, A. Olivier, V. Paolone, J. Park, G. N. Perdue, M. A. Ramírez, R. D. Ransome, H. Ray, D. Rimal, P. A. Rodrigues, D. Ruterbories, H. Schellman, C. J. Solano Salinas, H. Su, M. Sultana, V. S. Syrotenko, B. Yaeggy, and L. Zazueta. Constraint of the MINERνa medium energy neutrino flux using neutrino-electron elastic scattering. *Phys. Rev. D*, 100: 092001, Nov 2019. doi:10.1103/PhysRevD.100.092001.

[86] Erin Ewart. Primary and Secondary Vertexing Update for February 2024 Collaboration Meeting. NOVA Document 61190, February 2024. URL https://nova-docdb.fnal.gov/cgi-bin/sso/ShowDocument?docid=61190. NOvA internal document.

[87] Leonidas Aliaga, Derek Doyle, Matthew Judah, Norm Buchanan, Linda Cremonesi, Mat Muether, and Jon Paley. Measurement of the Double-Differential Inclusive Electron-Neutrino Charged-Current Cross Section in the NOvA Near Detector. NOVA Document 37668, 04 2020. URL https://nova-docdb.fnal.gov/cgi-bin/sso/ShowDocument?docid=37668. NOvA technical note.

[88] Andreas Hoecker, Peter Speckmayer, Joerg Stelzer, Jan Therhaag, Eckhard von Toerne, and Helge Voss. TMVA: Toolkit for Multivariate Data Analysis. *PoS*, ACAT:040, 2007.